RESEARCH ARTICLE

Sepsis leads to lasting changes in phenotype and function of memory CD8 T cells

Isaac J Jensen[1], Xiang Li[2], Patrick W McGonagill[3], Qiang Shan[4], Micaela G Fosdick[5], Mikaela M Tremblay[6], Jon CD Houtman[5,6], Hai-Hui Xue[4], Thomas S Griffith[7,8,9,10,11], Weiqun Peng[2], Vladimir P Badovinac[1,6]*

[1]Department of Pathology, University of Iowa, Iowa City, United States; [2]Department of Physics, The George Washington University, Washington, United States; [3]Department of Surgery, University of Iowa, Iowa City, United States; [4]Center for Discovery and Innovation, Hackensack University Medical Center, Nutley, United States; [5]Interdisciplinary Graduate Program in Molecular Medicine, University of Iowa, Iowa City, United States; [6]Interdisciplinary Graduate Program in Molecular Medicine, University of Iowa, Iowa City, United States; [7]Microbiology, Immunology, and Cancer Biology PhD Program, University of Minnesota, Minneapolis, United States; [8]Department of Urology, University of Minnesota, Minneapolis, United States; [9]Center for Immunology, University of Minnesota, Minneapolis, United States; [10]Masonic Cancer Center, University of Minnesota, Minneapolis, United States; [11]Minneapolis VA Health Care System, Minneapolis, United States

Abstract The global health burden due to sepsis and the associated cytokine storm is substantial. While early intervention has improved survival during the cytokine storm, those that survive can enter a state of chronic immunoparalysis defined by transient lymphopenia and functional deficits of surviving cells. Memory CD8 T cells provide rapid cytolysis and cytokine production following re-encounter with their cognate antigen to promote long-term immunity, and CD8 T cell impairment due to sepsis can pre-dispose individuals to re-infection. While the acute influence of sepsis on memory CD8 T cells has been characterized, if and to what extent pre-existing memory CD8 T cells recover remains unknown. Here, we observed that central memory CD8 T cells (T_{CM}) from septic patients proliferate more than those from healthy individuals. Utilizing LCMV immune mice and a CLP model to induce sepsis, we demonstrated that T_{CM} proliferation is associated with numerical recovery of pathogen-specific memory CD8 T cells following sepsis-induced lymphopenia. This increased proliferation leads to changes in composition of memory CD8 T cell compartment and altered tissue localization. Further, memory CD8 T cells from sepsis survivors have an altered transcriptional profile and chromatin accessibility indicating long-lasting T cell intrinsic changes. The sepsis-induced changes in the composition of the memory CD8 T cell pool and transcriptional landscape culminated in altered T cell function and reduced capacity to control *L. monocytogenes* infection. Thus, sepsis leads to long-term alterations in memory CD8 T cell phenotype, protective function and localization potentially changing host capacity to respond to re-infection.

***For correspondence:** vladimir-badovinac@uiowa.edu

Competing interest: The authors declare that no competing interests exist.

Funding: See page 26

Received: 04 June 2021
Accepted: 14 October 2021
Published: 15 October 2021

Reviewing Editor: Gabrielle T Belz, The University of Queensland, Australia

Introduction

Dysregulated systemic inflammatory responses define septic events and the associated cytokine storm, which is comprised of both pro- and anti-inflammatory cytokines (***CDC, 2020***; ***Singer et al., 2016***). Sepsis leads to a substantial global health and economic burden wherein nine people develop

eLife digest A dirty cut, a nasty burn, a severe COVID infection; there are many ways for someone to develop sepsis. This life-threatening condition emerges when the immune system overreacts to a threat and ends up damaging the body.

Even when patients survive, they are often left with a partially impaired immune system that cannot adequately protect against microbes and cancer; this is known as immunoparalysis. Memory CD8 T cells, a type of immune cell that is compromised by sepsis, are a long-lived population of cells that 'remember' previous infection or vaccination, and then react faster to prevent the same illness if the person ever encounters the same threat again. Yet it is unclear how exactly sepsis harms the function and representation of memory CD8 T cells, and the immune system in general.

Jensen et al. investigated this question, first by showing that sepsis leads to a profound loss of memory CD8 T cells, but that surviving memory CD8 T cells multiply quickly – especially a subpopulation known as central memory CD8 T cells – to re-establish the memory CD8 T cell population. Since the central memory CD8 T cells proliferate better than the other memory T cells this alters the overall composition of the pool of memory CD8 T cells, with central memory cells becoming overrepresented.

Further experiments revealed that this biasing toward central memory T cells, due to sepsis, created long-term changes in the distribution of memory CD8 T cells throughout the body. The way the genetic information of these cells was packaged had also been altered, as well as which genes were switched on or off. Overall, these changes reduced the ability of memory CD8 T cells to control infections.

Together, these findings help to understand how immunoparalysis can emerge after sepsis, and what could be done to correct it. These findings could also be applied to other conditions – such as COVID-19 – which may cause similar long-term changes to the immune system.

sepsis every 6 s and two of those individuals die (***Rudd et al., 2020***). In the United States alone the cost to treat sepsis is >$20 billion with a mortality rate of ~20 % (***CDC, 2020***). While a 20 % mortality rate is high, it is also a vast improvement over the last 30 years where mortality had been at ~50 % (***Dombrovskiy et al., 2007***; ***Gaieski et al., 2013***). This reduction in mortality rate has largely been through early intervention as the complexity of the cytokine storm has, dishearteningly, lead to the failure of >100 phase II and III clinical trials targeting the pro-inflammatory aspects of the cytokine storm (***Marshall, 2014***). Yet, even as survival of the cytokine storm has increased it has also become apparent that previously septic individuals are still at increased risk for mortality, this defines the sepsis-induced immunoparalysis state (***Delano and Ward, 2016a***; ***Delano and Ward, 2016b***; ***Dombrovskiy et al., 2007***; ***Donnelly et al., 2015***).

Sepsis-induced immunoparalysis is characterized by an increased susceptibility to both new and previously encountered unrelated infections and cancer (***Danahy et al., 2019***; ***Jensen et al., 2018a***; ***Kutza et al., 1998***; ***Walton et al., 2014***). Alternately, sepsis-induced immunoparalysis reduces susceptibility to development of autoimmunity, cumulatively demonstrating immunologic impairment (***Jensen et al., 2020***). These profound impairments are sufficient to reduce the 5 year survival of septic cohorts, relative to non-septic cohorts; consequently, the majority of sepsis-associated mortality is late mortality secondary to the cytokine storm (***Dombrovskiy et al., 2007***; ***Donnelly et al., 2015***; ***Gaieski et al., 2013***). This immunologic impairment is typified by transient lymphopenia and reduced capacity of various surviving lymphocyte populations to perform effector function (***Hotchkiss et al., 2016***; ***Hotchkiss et al., 2013***), including CD4 (***Cabrera-Perez et al., 2014***; ***Cabrera-Perez et al., 2015***; ***Chen et al., 2017***; ***Jensen et al., 2020***; ***Martin et al., 2020***; ***Sjaastad et al., 2020b***) and CD8 T cells (***Condotta et al., 2013***; ***Danahy et al., 2017***; ***Danahy et al., 2019***; ***Duong et al., 2014***; ***Serbanescu et al., 2016***; ***Xie et al., 2019***), B cells (***Hotchkiss et al., 2001***; ***Sjaastad et al., 2018***; ***Unsinger et al., 2010***), NK cells (***Hou et al., 2014***; ***Jensen et al., 2021b***; ***Jensen et al., 2018b***; ***Souza-Fonseca-Guimaraes et al., 2012***), and dendritic cells (DCs) (***Poehlmann et al., 2009***; ***Roquilly et al., 2017***; ***Strother et al., 2016***). We and others have characterized numerous impairments early after sepsis induction; however, the extent to which those cell populations recover in number and function remains largely unknown.

Specifically, sepsis-induced lymphopenia impacts both memory and naïve CD8 T cells early after sepsis (***Condotta et al., 2015***; ***Condotta et al., 2013***; ***Duong et al., 2014***; ***Jensen et al., 2018a***; ***Markwart et al., 2014***). Additionally, those memory CD8 T cells that survive the cytokine storm are less capable of undergoing antigen-dependent effector function and responding to inflammatory cues (bystander activation). These intrinsic impairments, in conjunction with the numeric deficits imposed by the lymphopenic environment, reduce host capacity to control both infection (i.e. viral and bacterial) and cancer (***Danahy et al., 2017***; ***Danahy et al., 2019***; ***Duong et al., 2014***; ***Gurung et al., 2011***). Additionally, extrinsic factors, such as reduced integrin expression on endothelia (***Danahy et al., 2017***) or altered monocyte/ macrophage activity (***Jensen et al., 2021a***; ***Roquilly et al., 2020***), can influence CD8 T cell capacity to migrate into sites of infection. Even when T cells are spared from the cytokine storm by vascular exclusion (i.e. tissue residence) CD8 T cell-mediated protection can be hampered by inability of other cells (e.g. endothelia) to respond to the inflammatory cues provided by CD8 T cells (***Danahy et al., 2017***). Yet, these impairments are largely characterized proximal to the septic insult. However, sepsis-induced impairments are long-lasting and may not be consistent across time (***Jensen et al., 2018a***). Specifically, the lymphopenic environment is transient yet the ability to control cancer can remain reduced long after numeric recovery is complete (***Danahy et al., 2019***). Thus, while there does not appear to be preferential susceptibility to sepsis, if and how different subsets of memory CD8 T cells recover may dramatically shape how hosts respond to pathogen re-encounter and thereby contribute to the immunoparalysis state.

Here, using samples from septic patients and well described experimental models we demonstrate increased proliferation of CD8 T cells (particularly central memory cells [T_{CM}]) in septic patients and mice after cecal ligation and puncture (CLP)-induced sepsis, relative to non-septic controls. As a consequence of this increased proliferation, there is a remodeling of the memory CD8 T cell pool. This compositional change in turn leads to lasting changes in the localization, function, and protective capacity of pre-existing memory CD8 T cells.

Results

Increased CD8 T cell proliferation in septic patients

The sepsis-induced immunoparalysis state poses a substantial threat to the health and long-term survival of septic patients (***Delano and Ward, 2016a***; ***Delano and Ward, 2016b***; ***Dombrovskiy et al., 2007***; ***Donnelly et al., 2015***). A major contributing factor to sepsis-induced immunoparalysis is the intrinsic and numerical deficits imposed on naive and memory CD8 T cells (***Jensen et al., 2018a***). In particular, deficits in existing memory CD8 T cells can enhance host susceptibility to pathogens against which the host was previously immune or vaccinated. To understand how CD8 T cells respond to septic insult and the lymphopenic state, septic patients were recruited within 24 hr of admission and the frequency and number of CD8 T cells in the peripheral blood were compared to that of healthy controls. Patient cohorts did not exhibit substantial demographic differences though septic patients were severely ill, as defined by APACHE II and SOFA scores (***Table 1***). While there was not a difference in the frequency of CD8 T cells among lymphocytes between septic patients and healthy controls (***Figure 1a and b***), there was a cohort of septic patients with a substantially reduced number of CD8 T cells per mL of blood (***Figure 1c***) reflecting the sepsis-induced lymphopenia. It is relevant to consider that admission time may not correspond to the onset of sepsis such that admitted patients may have not yet experienced or already recovered from sepsis-associated lymphopenia. Thus, numeric variability in samples may reflect a broad range of insult and recovery within the 24 hr of admission. Notably, robust induction of Ki67 expression, a marker of recent proliferation, by CD8 T cells (***Figure 1a and d***) was observed, regardless of degree of lymphopenia.

Table 1. Patient demographics.

Patients	Septic (n = 27)	Control (n = 16)	p-value
Age (mean ± SD)	59.3±16.3	51.6±13.2	ns
Male (%)	40.7%	37.5%	ns
Caucasian (%)	100%	81.3%	0.0454
APACHE II Score (mean ± SD)	11.1±5.9		
SOFA Score (mean ± SD)	4.6±4.3		
% in Septic Shock	55.6%		
Time Post-Admission (hrs)	6.1±5.6		

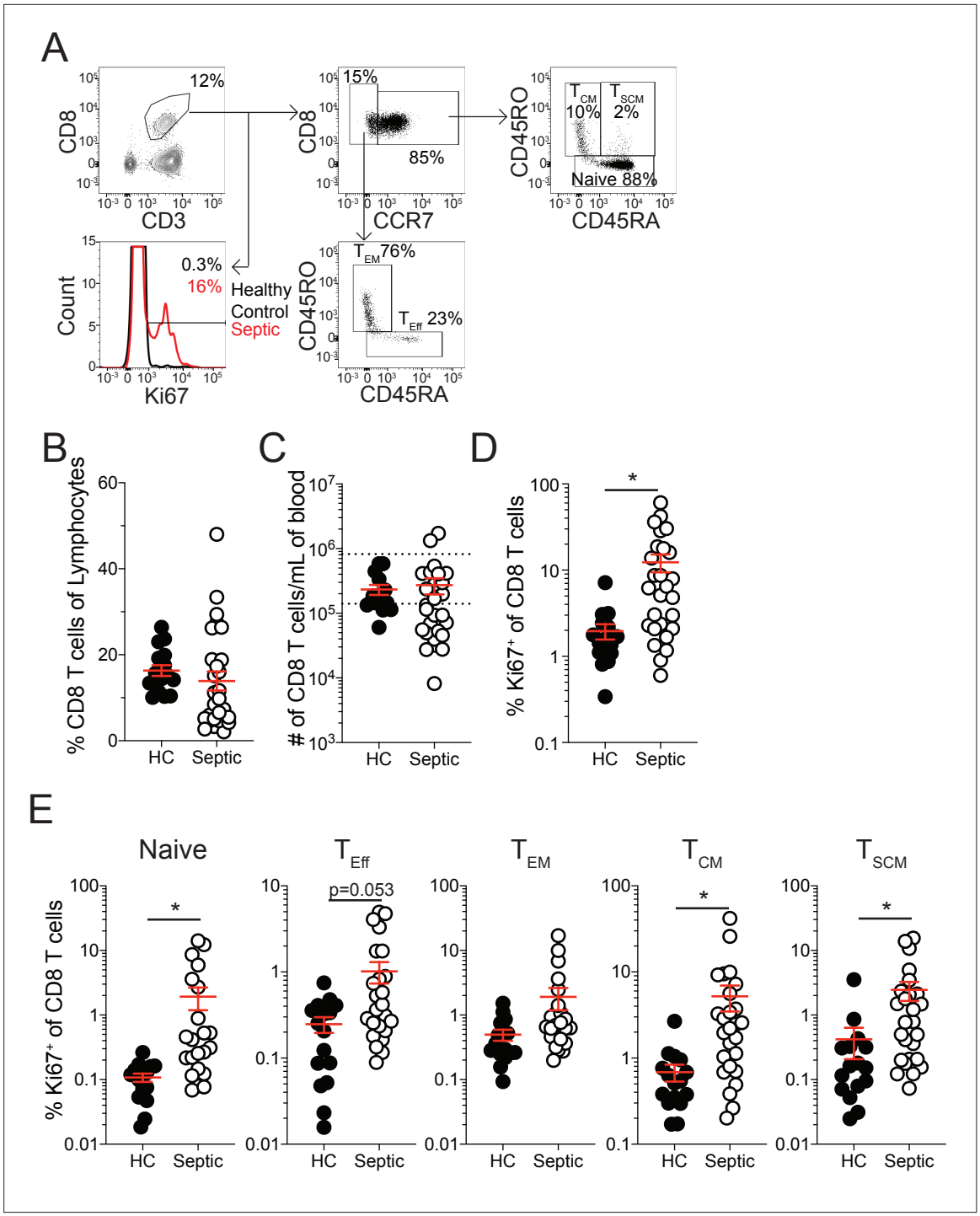

Figure 1. Increased proliferation among CD8 T cells of septic patients. (**A**) Representative gating for CD8 T cell subsets and Ki67 expression from healthy controls and septic patients (within 24 hr of hospital admission). (**B**) Frequency and (**C**) number of CD8 T cells among lymphocytes in healthy controls and septic patients. Dashed lines indicate the normal range for the number of CD8 T cells per mL of blood. (**D**) Frequency of Ki67 expressing CD8 T cells in healthy controls and septic patients. (**E**) Frequency Ki67 expressing cells among Naïve, Effector (T_{Eff}), Effector Memory (T_{EM}), Central Memory (T_{CM}), and Stem Cell Memory (T_{SCM}) CD8 T cells from healthy controls and septic patients. Data are representative of 2 independent experiments with 16–27 patients per group. *=p < 0.05. Error bars in represent standard error of the mean.

The online version of this article includes the following figure supplement(s) for figure 1:

Source data 1. Source data for ***Figure 1***.

Figure supplement 1. Composition of total and proliferating CD8 T cells in healthy controls and septic hosts.

Figure supplement 1—source data 1. Source data for ***Figure 1—figure supplement 1***.

This proliferation could either represent newly evoked effector CD8 T cell responses to the sepsis-inducing pathogens or homeostatic proliferation of surviving T cells induced by lymphopenic environment (***Cheung et al., 2009***; ***Davenport et al., 2019***; ***Jensen et al., 2018a***; ***Unsinger et al., 2009***). To address this, the frequency of Ki67 expressing cells was evaluated between naïve ($CCR7^+CD45RA^+CD45RO^-$), effector (T_{Eff}; $CCR7^-CD45RA^+CD45RO^-$), effector memory (T_{EM}; $CCR7^-CD45RA^-CD45RO^+$), central memory (T_{CM}; $CCR7^+CD45RA^-CD45RO^+$), and stem cell memory (T_{SCM}; $CCR7^+CD45RA^+CD45RO^+$) CD8 T cells (***Cieri et al., 2013***; ***Sarkar et al., 2019***). If the proliferation was in response to the septic insult only T_{Eff} CD8 T cells should be prominently proliferating relative to healthy controls; however, there was only modest induction of Ki67 among T_{Eff} CD8 T cells (***Figure 1e***). Intriguingly, robust proliferation among naïve, T_{CM}, and T_{SCM} CD8 T cells was observed, suggesting proliferation may reflect numerical recovery after sepsis-induced lymphopenia (***Figure 1e***). Notably, there was not a significant increase in $Ki67^+$ T_{EM} CD8 T cells from septic patients (***Figure 1e***). These data suggest that there is differential proliferation by memory CD8 T cell subsets in septic hosts. Given this differential proliferation by memory CD8 T cell subsets, an altered composition of the memory CD8 T cell pool would be anticipated after sepsis. Indeed, there was a modest, although not statistically different, increase in the frequency of both T_{CM} and T_{SCM} CD8 T cells in septic patients, relative to healthy controls, even at this early time point (***Figure 1—figure supplement 1a***). Importantly, when evaluating the representation of CD8 T cell subsets among Ki67-expressing CD8 T cells, T_{CM} and T_{SCM} CD8 T cells were not proportionally increased (***Figure 1—figure supplement 1b***), with T_{CM} being the most prominent among cells that recently proliferated. Collectively, these data suggest that sepsis may alter the composition of the memory CD8 T cell compartment due to intrinsic differences in the capacity of different memory CD8 T cell subsets to proliferate.

Pre-existing memory 8 T cells numerically recover after sepsis

To further address how sepsis may alter the composition of the CD8 T cell compartment due to differential capacity memory CD8 T cell subsets to sense signals of the 'empty' environment and undergo homeostatic proliferation, we utilized a murine LCMV-infection model to establish memory CD8 T cells followed by a cecal ligation and puncture (CLP; ***Figure 2a***). To facilitate resolution/analyses of the memory CD8 T cell compartment a physiologically relevant number of naïve $Thy1.1^+$ TCR-Tg P14 CD8 T cells, specific for the GP_{33} epitope of LCMV, were adoptively transferred into $Thy1.2^+$ recipient mice. Mice were then infected with LCMV-Arm, an acute infection which elicits a robust and well characterized memory CD8 T cell response (***Badovinac et al., 2007***). This system of memory generation and sepsis induction enables rigorous interrogation of a defined population of "pre-existing" memory CD8 T cells (memory cells that exist prior to sepsis induction) wherein both the time of the priming infection and septic event are known. Additionally, naïve and antigen-experienced (Ag-exp) CD8 T cells can be differentiated based on the expression of surrogate markers of activation CD8a and CD11a (naïve: $CD8a^{hi}CD11a^{lo}$; Ag-exp: $CD8a^{lo}CD11a^{hi}$) (***Rai et al., 2009***). This enables evaluation of endogenous naïve and Ag-exp CD8 T cells in addition to the Ag-exp P14 CD8 T cells (***Figure 2b***). Further depth of interrogation is achieved with memory P14 CD8 T cells, relative to the bulk antigen-experienced CD8 T cell population, given that memory P14 CD8 T cells are not specific for antigens evoked/released during the septic event, and the influence of sepsis on this discrete pre-existing memory CD8 T cell population delineates from potential 'secondary' antigen encounter and from potential and anticipated novel Ag-specific CD8 T cell responses to the septic event.

Following septic insult, the lymphopenic state impacted naïve and Ag-exp cells to the same degree (***Figure 2c***), as has been previously reported (***Condotta et al., 2013***; ***Duong et al., 2014***; ***Jensen et al., 2018a***). Importantly, the memory P14 CD8 T cells were similarly susceptible to sepsis-induced lymphopenia as the endogenous Ag-exp cells (***Figure 2c***). Additionally, there was induction of Ki67 expression by memory P14 CD8 T cells after sepsis (***Figure 2d and e***), demonstrating that the P14 CD8 T cells can be used to model the influence of sepsis on pre-existing memory CD8 T cells. When the number of memory P14 CD8 T cells per mL of blood was quantified, we observed numeric loss and recovery of P14 CD8 T cells in CLP hosts (***Figure 2f***), similar to prior reports of homeostatic proliferation following sepsis-induced lymphopenia (***Unsinger et al., 2009***). Thus, pre-existing memory CD8 T cells numerically recover with time after sepsis, potentially due to increased proliferation in response to the sepsis-induced lymphopenic environment.

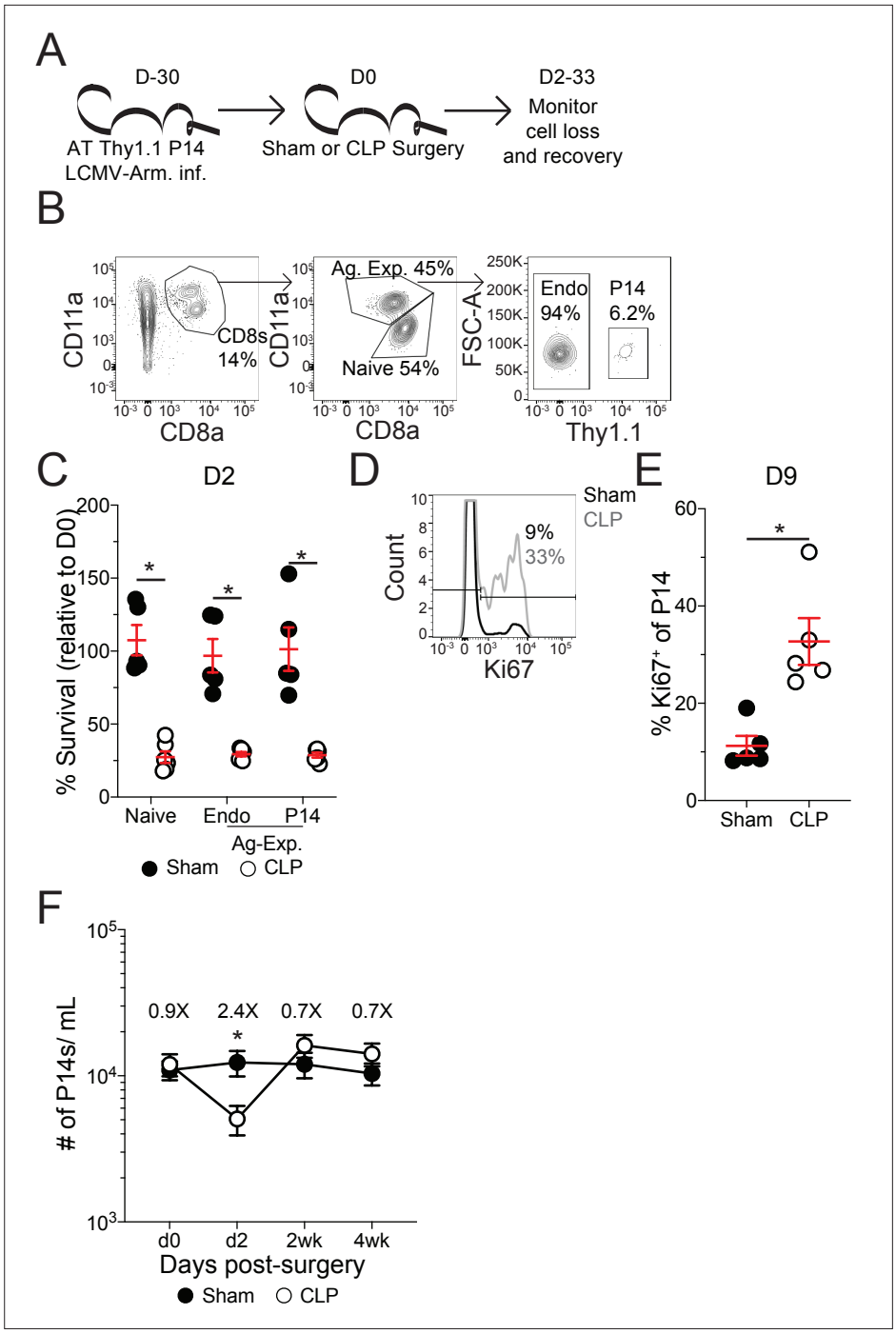

Figure 2. Pre-existing memory CD8 T cells numerically recover with time after sepsis. (**A**) Experimental Design: Antigen-experienced P14 chimeric mice were generated by adoptive transfer of 5 × 10^3 naïve Thy1.1$^+$ TCR-transgenic P14 CD8 T cells to Thy1.2$^+$ C57Bl/6 mice that were subsequently infected with LCMV-Armstrong (LCMV-Arm). Mice underwent Sham or CLP surgery 30 days after infection. The number of endogenous naïve, endogenous antigen-experienced, and antigen-experienced P14 CD8 T cells was monitored in the blood. (**B**) Representative gating for endogenous naïve, endogenous antigen-experienced, and antigen-experienced P14 CD8 T cells. (**C**) Percent survival of endogenous naïve, endogenous antigen-experienced, and antigen-experienced P14 CD8 T cells in the blood 2 days after either Sham or CLP surgery, relative to a pre-surgery bleed. (**D**) Representative gating of Ki67 on P14 CD8 T cells. (**E**) Frequency of Ki67-expressing P14 CD8 T cells in the blood of Sham and CLP hosts 9 days post-surgery. (**F**) The number of P14 CD8 T cells per mL of blood in Sham and CLP hosts prior to (d0), or 2 days (d2), 2 weeks (2 wk), and 4 weeks (4 wk) after surgery. Values above the bars indicate

Figure 2 continued on next page

Figure 2 continued

the fold difference (Sham/CLP) in the number of P14 CD8 T cells. (**C–E**) Are representative of 3 independent experiments with 5–6 mice per group. (**F**) Is cumulative from two independent experiments with 10–12 mice per group. *=p < 0.05. Error bars represent standard error of the mean.

The online version of this article includes the following figure supplement(s) for figure 2:

Source data 1. Source data for ***Figure 2C***.

Source data 2. Source data for ***Figure 2E***.

Source data 3. Source data for ***Figure 2F***.

Numeric recovery following sepsis increases the proportion of central memory CD8 T cells

To address how this numeric recovery may alter the composition of the memory T cell compartment phenotypic characterization of splenic memory P14 CD8 T cells from Sham and CLP mice was performed >30 days post-surgery (***Figure 3a***). Additionally, FlowSOM was utilized to cluster memory P14 CD8 T cells based on surface marker expression of CD8a, CD11a, Thy1.1, CD62L, KLRG1, CD127, CX3CR1, CXCR3, CD25, CD27, CD69, CD103, and CD122 in an unbiased manner (***Van Gassen et al., 2015***). Memory P14 CD8 T cells were similarly evaluated by tSNE analysis and FlowSOM-defined clusters were then projected into the tSNE (***Figure 3b and c***). Notably, Sham and CLP hosts had differential representation of two of the most prominent clusters (6 and 8) with cluster six being enriched in Sham P14 CD8 T cells and cluster eight in CLP P14 CD8 T cells (***Figure 3d and e***). Clusters 6 and 8 were then compared to define distinctions between Sham and CLP cells (***Figure 3g***). Memory P14 CD8 T cells enriched in Sham mice (cluster 6) were CD62L^{-}KLRG1^{+}CD127^{-}CX3CR1^{+}CXCR3^{lo}, while memory P14 CD8 T cells enriched in CLP mice (cluster 8) were CD62L^{+}KLRG1^{-}CD127^{+}CX3CR1^{-}CXCR3$^{lo/med}$ (***Figure 3h***). Clusters 6 and 8 therefore appear to define T_{EM} and T_{CM} CD8 T cells, respectively. Definition of these subsets was predominantly by the expression of CD62L, although the expression of KLRG1, CD127, CX3CR1, and CXCR3 conformed with the respective phenotypes as well (***Martin and Badovinac, 2018***). Thus, CLP P14 CD8 T cells are enriched for T_{CM} with a reduced representation of T_{EM}, corresponding to the increased proliferation of CD8 T_{CM} observed in septic patients (***Figure 1e***; ***Figure 1—figure supplement 1b***).

T_{CM} have a higher capacity to undergo homeostatic proliferation, relative to T_{EM}, which accounts for the gradual shift toward T_{CM} with time after antigen encounter (***Martin and Badovinac, 2018***; ***Martin et al., 2015***; ***Wherry et al., 2003***). Therefore, to address whether the higher proliferative potential of T_{CM} accounted for the shift to CD8 T_{CM} following sepsis, Ki67 expression in splenic T_{EM} and T_{CM} P14 CD8 T cells was interrogated at various times after Sham or CLP surgery (***Figure 4a***). Indeed, both T_{CM} and T_{EM} proliferated in CLP hosts greater than their Sham counterparts, following lymphopenia (***Figure 4b***). However, P14 CD8 T_{CM} cells proliferated more robustly than their T_{EM} counterparts in CLP hosts. Importantly, P14 CD8 T_{CM} cells proliferated more than their T_{EM} counterparts in Sham hosts across all timepoints, consistent with prior reports of higher homeostatic proliferation among T_{CM} cells (***Wherry et al., 2003***). To confirm the higher degree of proliferation in P14 CD8 T_{CM} cells following sepsis, BrdU incorporation was evaluated over the course of a week beginning at D9 post-surgery, the timepoint at which differential proliferation had been observed by Ki67 expression (***Figure 4c***). Similar to the results with Ki67, elevated proliferation was observed in both T_{CM} and T_{EM} P14 CD8 T cells from CLP hosts, relative to Sham hosts (***Figure 4d***). Additionally, P14 CD8 T_{CM} cells had higher incorporation of BrdU (relative to T_{EM} counterparts) in both Sham and CLP hosts with P14 CD8 T_{CM} cells from CLP hosts having the highest degree of BrdU incorporation. Similar results were also demonstrated in endogenous Ag-exp CD8 T cells reaffirming the findings in the TCR-Tg memory P14 CD8 T cells. This proliferative difference was further associated with an increase in the frequency of T_{CM} among P14 CD8 T cells at D16 post-surgery, the time at which BrdU assessment was performed (***Figure 4e***). Additionally, a trending increase in the representation of T_{CM} was observed among Ag-exp CD8 T cells in CLP hosts, relative to Sham hosts, at the same time in spite of potential novel effector CD8 T cell responses to the septic insult.

In addition to differential capacity to undergo homeostatic proliferation T_{CM} and T_{EM} have different localization throughout the body. T_{CM} preferentially localizes to lymphatic tissue while T_{EM} preferentially circulates and traverse non-lymphatic tissue (***Gerlach et al., 2016***; ***Masopust et al., 2001***;

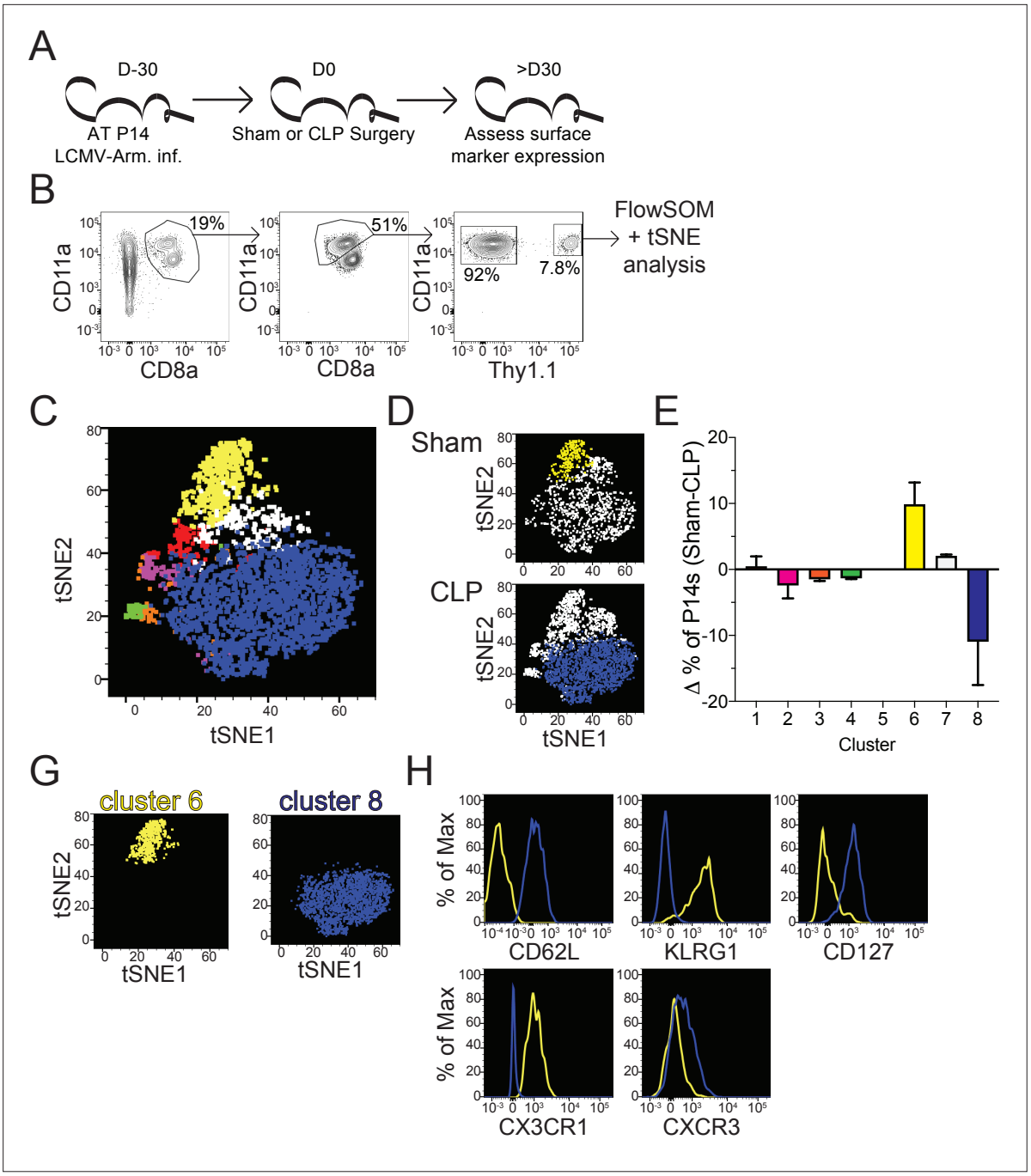

Figure 3. Sepsis alters the phenotypic composition of pre-existing memory CD8 T cells. (**A**) Experimental Design: Antigen-experienced P14 chimeric mice were generated by adoptive transfer of 5 × 10^3 naive Thy1.1$^+$ TCR-transgenic P14 CD8 T cells to Thy1.2$^+$ CD57Bl/6 mice that were subsequently infected with LCMV-Armstrong (LCMV-Arm). Mice underwent Sham or CLP surgery 30 days after infection. Phenotypic marker expression on P14 CD8 T cells was then assessed 30 days after surgery. (**B**) Representative antigen-experienced P14 CD8 T cells used in FlowSOM and tSNE analyses. (**C**) tSNE displaying FlowSOM defined clusters among P14 CD8 T cells based on surface marker expression of CD8a, CD11a, Thy1.1, CD62L, KLRG1, CD127, CX3CR1, CXCR3, CD25, CD27, CD69, CD103, and CD122. (**D**) Sham and CLP tSNE plots displaying clusters most robustly enriched in corresponding group. (**E**) Change (Δ) in the frequency of P14 CD8 T cells in each cluster (Sham-CLP); clusters biased toward Sham are >0, clusters biased toward CLP are <0. (**G**) tSNE plots displaying the clusters 6 (enriched in Sham hosts) and 8 (enriched in CLP hosts). (**H**) Surface expression of CD62L, KLRG1, CD127, CX3CR1, and CXCR3 comparing clusters 6 and 8. Data are representative of two independent experiments with 2–3 mice per group. Error bars indicate standard error of the mean.

The online version of this article includes the following figure supplement(s) for figure 3:

Source data 1. Source data for ***Figure 3***.

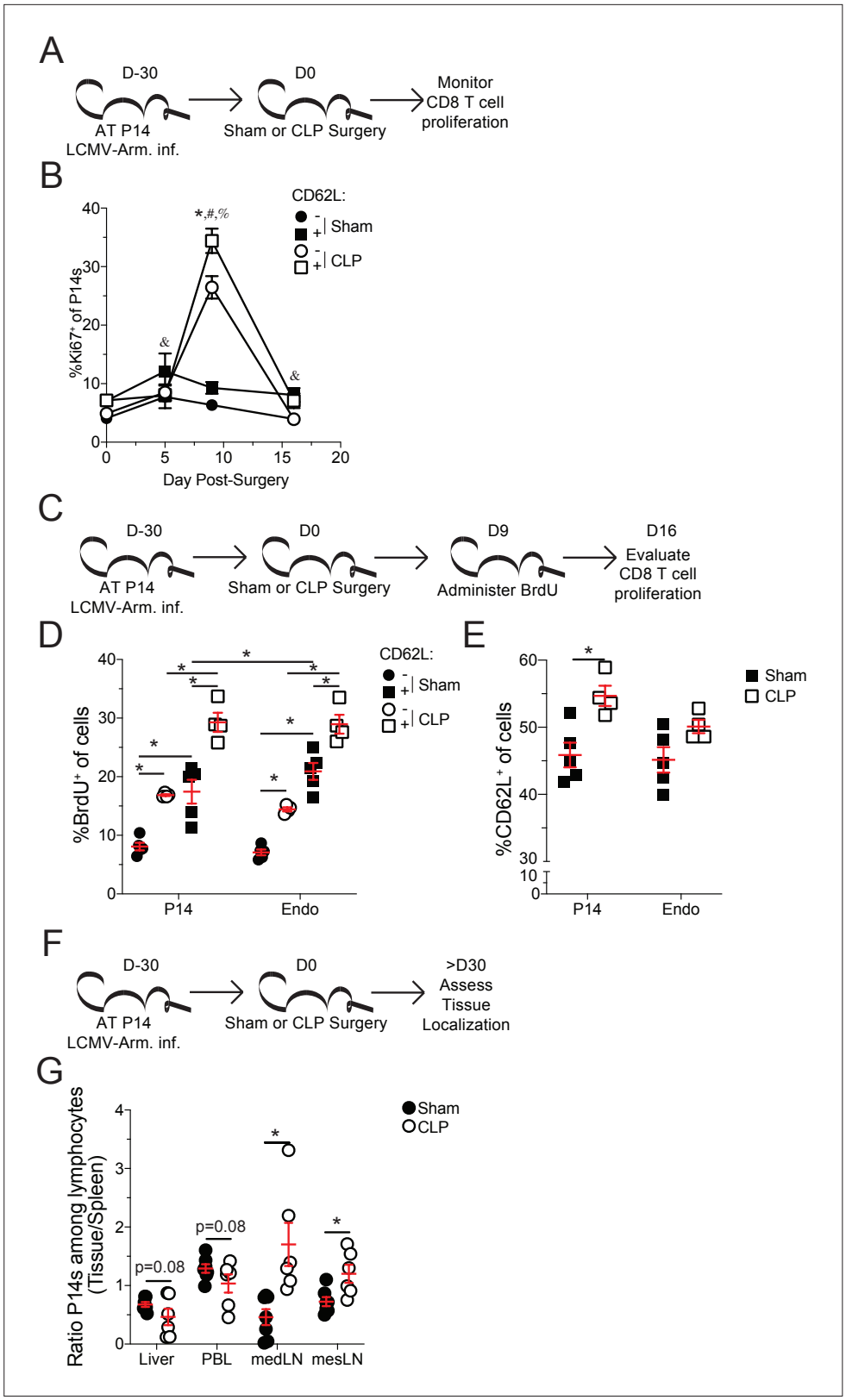

Figure 4. Central memory CD8 T cells more robustly proliferate after sepsis. (**A**) Experimental Design: Antigen-experienced P14 chimeric mice were generated by adoptive transfer of 5 × 10^3 naive Thy1.1$^+$ TCR-transgenic P14 CD8 T cells to Thy1.2$^+$ C57Bl/6 mice that were subsequently infected with LCMV-Armstrong (LCMV-Arm). Mice underwent Sham or CLP surgery 30 days after infection. The frequency of Ki67 expressing central and effector

Figure 4 continued on next page

Figure 4 continued

memory P14 CD8 T cells was monitored in the spleen after surgery. (**B**) Frequency of Ki67 expressing cells among central ($CD62L^+$) and effector ($CD62L^-$) memory P14 CD8 T cells in Sham and CLP hosts prior to (d0) or 5-, 9-, and 16 days after surgery. *=$p < 0.05$ $CD62L^+$ v $CD62L^-$ CLP P14 CD8 T cells; &=$p < 0.05$ $CD62L^+$ v $CD62L^-$ Sham P14 CD8 T cells; #=$p < 0.05$ Sham v CLP $CD62L^+$ P14 CD8 T cells; %=$p < 0.05$ Sham v CLP $CD62L^-$ P14 CD8 T cells (**C**) Experimental Design: Antigen-experienced P14 chimeric mice were generated by adoptive transfer of 5×10^3 naïve $Thy1.1^+$ TCR-transgenic P14 CD8 T cells to $Thy1.2^+$ C57Bl/6 mice that were subsequently infected with LCMV-Arm. Mice underwent Sham or CLP surgery 30 days after infection followed by BrdU administration 9 days later. BrdU incorporation by central and effector memory endogenous and P14 CD8 T cells was assessed 7 days later. (**D**) Frequency of $CD62L^+$ and $CD62L^-$ memory P14 CD8 T cells and endogenous CD8 T cells that have incorporated BrdU. (**E**) Frequency of $CD62L^+$ P14 CD8 T cells and endogenous CD8 T cells 16 days after surgery. (**F**) Experimental Design: Antigen-experienced P14 chimeric mice were generated by adoptive transfer of 5×10^3 naive $Thy1.1^+$ TCR-transgenic P14CD8 T cells to $Thy1.2^+$ C57Bl/6 mice that were subsequently infected with LCMV-Arm. Mice underwent Sham or CLP surgery 30 days after infection. The frequency of P14 CD8 T cells among lymphocytes in the spleen, liver, PBL, mediastinal lymph node (medLN), and mesenteric lymph node (mesLN) was then determined 30 days after surgery. Preferential localization was determined by the ratio of P14 CD8 T cells in the tissues compared relative to the spleen. (**G**) Ratio of the frequency of P14 CD8 T cells among lymphocytes in the liver, PBL, medLN, and mesLN relative to the spleen. All data are representative of at least two independent experiments with 4–8 mice per group. *=$p < 0.05$. Error bars represent standard error of the mean.

The online version of this article includes the following figure supplement(s) for figure 4:

Source data 1. Source data for ***Figure 4B***.

Source data 2. Source data for ***Figure 4D and E***.

Source data 3. Source data for ***Figure 4G***.

Mueller et al., 2013). To further address this shift in the representation of T_{CM} and T_{EM}, the localization of memory P14 CD8 T cells was evaluated in the liver, peripheral blood lymphocytes (PBL), mediastinal lymph nodes (mLN), and mesenteric lymph nodes (mesLN) relative to the spleen (***Figure 4f***). Spleen was chosen as the baseline for comparison as it is a mixture of circulation with lymphatic tissue. PBL was chosen to emphasize circulating cells, while liver was chosen as a non-lymphatic tissue because it is a highly vascular tissue with direct contact to blood coming from the abdominal cavity and thus relevant to the septic insult. MedLN are the site of initial infection with LCMV-Arm following i.p. infection and is therefore relevant to the generation of the initial memory response (***Olson et al., 2012***), while mesLN drain the gut tissue and are relevant to CLP induction. Thus, if sepsis leads to a global shift toward central memory we expected to see a reduced proportion of memory P14 CD8 T cells in the liver and PBL and a greater proportion in the medLN and mesLN in CLP hosts, relative to Sham. Indeed, the ratio of P14 CD8 T cells among lymphocytes in the liver and PBL, relative to the spleen, had a trending reduction in CLP hosts, compared to Sham hosts (***Figure 4g***). Conversely, the ratio of P14 CD8 T cells among lymphocytes in the medLN and mesLN relative to the spleen, were significantly increased in CLP hosts, compared to Sham hosts. These data demonstrate differential localization of CD8 T cells in Sham and CLP hosts corresponding to the change in the representation of T_{EM} and T_{CM}. Cumulatively, the data in ***Figure 4*** demonstrate that preferential proliferation by T_{CM} alters the composition and localization of pre-existing memory CD8 T cells after sepsis. Thus, pre-existing differences in the biology of central and effector memory T cells are the underlying mechanism by which central memory CD8 T cells become over-represented in pre-existing memory populations after sepsis.

Sepsis leads to long-term changes in memory CD8 T cell transcription and chromatin accessibility

Beyond localization T_{CM} and T_{EM} have differential functions mediated by discrete transcriptional and epigenetic landscapes (***Chang et al., 2014***; ***Kaech and Cui, 2012***; ***Milner et al., 2020***). Therefore, to address how the sepsis-induced changes in the composition of pre-existing memory CD8 T cells may alter the overall transcriptional regulation of memory CD8 T cells RNA-sequencing was performed on memory P14 CD8 T cells from Sham and CLP hosts both 1- and 31 days post-surgery (***Figure 5a***). Numerous transcriptional differences between the four groups were identified (***Figure 5b–d***). Notably, when evaluated by principal component analysis (PCA) there was clear distinction between the Sham and CLP groups at each timepoint (***Figure 5b***); however, this distinction narrowed at D31 relative to

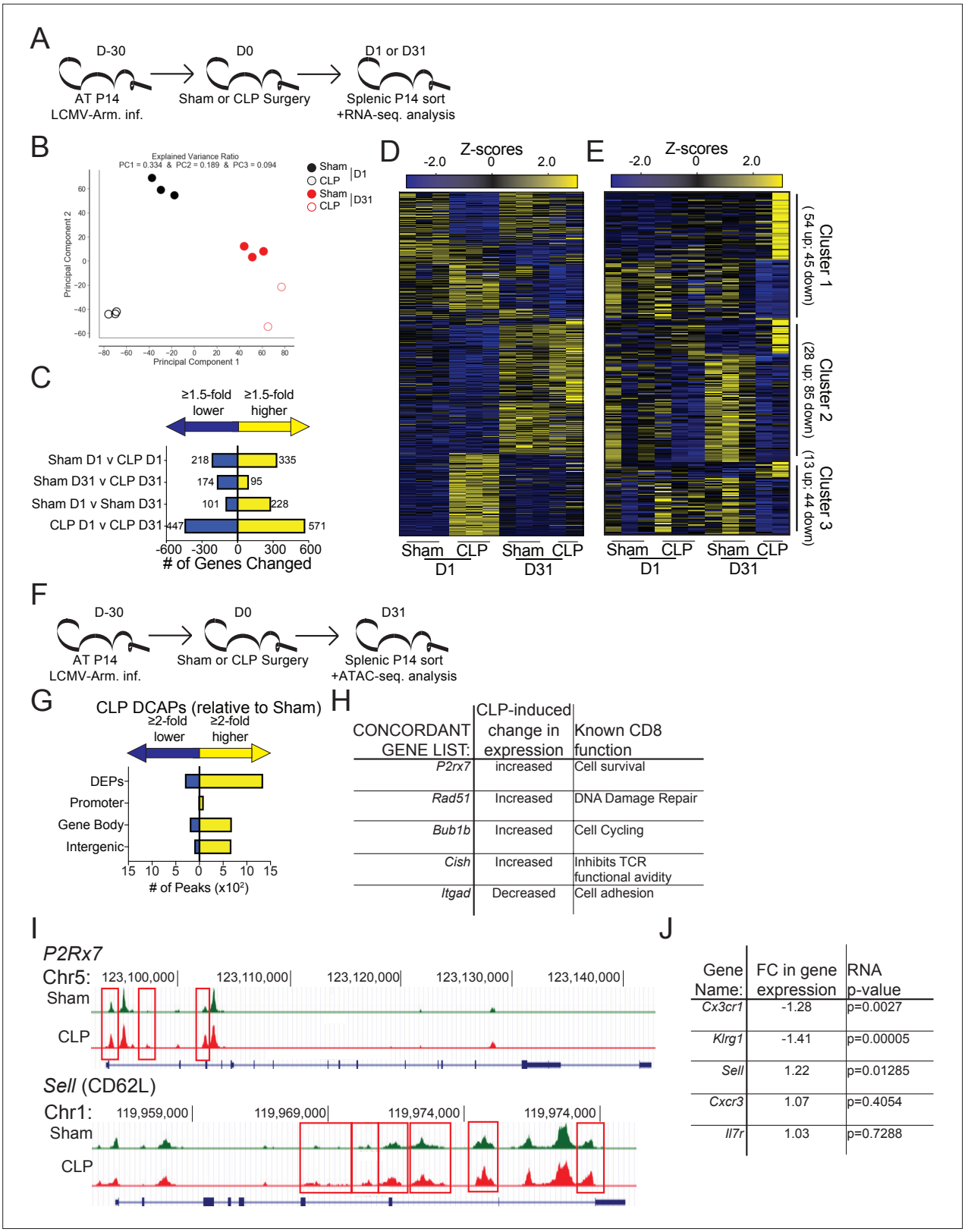

CONCORDANT GENE LIST:	CLP-induced change in expression	Known CD8 function
P2rx7	increased	Cell survival
Rad51	Increased	DNA Damage Repair
Bub1b	Increased	Cell Cycling
Cish	Increased	Inhibits TCR functional avidity
Itgad	Decreased	Cell adhesion

Gene Name:	FC in gene expression	RNA p-value
Cx3cr1	-1.28	p=0.0027
Klrg1	-1.41	p=0.00005
Sell	1.22	p=0.01285
Cxcr3	1.07	p=0.4054
Il7r	1.03	p=0.7288

Figure 5. Sepsis alters the gene expression and chromatin accessibility of pre-existing memory CD8 T cells. (**A**) Experimental Design: Antigen-experienced P14 chimeric mice were generated by adoptive transfer of 5 × 10^3 naive Thy1.1$^+$ TCR-transgenic P14 CD8 T cells to Thy1.2$^+$ C57Bl/6 mice that were subsequently infected with LCMV-Arm. Mice underwent Sham or CLP surgery 30 days after infection. Splenic P14 CD8 T cells were FACS-sorted one or 31 after surgery for RNA extraction. P14 CD8 T cells were isolated from 3 D1-Sham hosts, 3 D1-CLP hosts, 3 D31-Sham hosts, and 2 D31-

Figure 5 continued on next page

Figure 5 continued

CLP hosts. (**B**) Principal Component analysis of P14 CD8 T cells from Sham and CLP hosts either 1- or 31 days post-surgery. (**C**) Number of statistically significant gene changes as a result of indicated comparisons. (**D**) Gene expression heatmap of genes with statistically significant changes (fold change >1.5, $p < 0.05$) as a result of any comparison. (**E**) Gene expression heatmap of genes with statistically significant changes (fold change >1.5, $p < 0.05$) between D31 Sham and CLP P14 CD8 T cells. Clusters were consecutively defined by similar expressional changes in: D1 to D31 Sham P14 CD8 T cells and D31 Sham to CLP P14 CD8 T cells [Cluster 1], D1 Sham to CLP P14 CD8 T cells and D31 Sham to CLP P14 CD8 T cells [Cluster 2], and non-defined by prior categorization [Cluster 3] (**F**) Experimental Design: Antigen-experienced P14 chimeric mice were generated by adoptive transfer of 5×10^3 naive Thy1.1$^+$ TCR-transgenic P14 CD8 T cells to Thy1.2$^+$ C57Bl/6 mice that were subsequently infected with LCMV-Arm. Mice underwent Sham or CLP surgery 30 days after infection. Splenic P14 CD8 T cells were FACS-sorted 31 days after surgery for assessment of chromatin accessibility. P14 CD8 T cells were isolated from 2 D31-Sham hosts and 3 D31-CLP hosts. (**G**) Total number of differential chromatin accessibility peaks (DCAPs, fold change >2 $p < 0.05$) and delineation of those within either a promoter, gene body, or intergenic regions assigned to the most proximal to a transcription start site. (**H**) List of genes whose change in transcript is concordant with changes in chromatin accessibility along with the relative change and known function in CD8 T cells. (**I**) Example of differentially expressed peaks (indicated by the red box) within the *P2R×7* and *Sell* gene loci from representative Sham and CLP P14s. (**J**) List of genes whose expression defined the phenotypically distinct populations between Sham and CLP P14 CD8 T cells in ***Figure 3*** alongside their fold change in transcript and the p-value associated with that fold-change.

The online version of this article includes the following figure supplement(s) for figure 5:

Source data 1. Source data for ***Figure 5C and D***.

Source data 2. Source data for ***Figure 5E***.

D1 potentially reflecting some degree of recovery from the initial the cytokine storm. Additionally, D1 and D31 were distinct within their respective surgical groups recapitulating prior literature demonstrating how memory changes with time after antigen encounter (***Davenport et al., 2019***; ***Martin et al., 2017***). Importantly, numerous gene changes (269 total; 174 down, 95up) were present at D31 post-surgery in CLP hosts, relative to Sham controls (***Figure 5c and d***). To understand how these lasting transcriptional changes related to the septic insult, the significantly different genes expressed at D31 by Sham and CLP memory P14 CD8 T cells were clustered into three groups (***Figure 5e***). Given our observation of faster transition to central memory by CD8 T cells after sepsis the first cluster of genes identified were those that were similarly changed when comparing D1 to D31 Sham and D31 Sham to CLP P14 CD8 T cells. These changes constituted 99 of the 269 transcriptional (***Table 2***) differences between Sham and CLP memory P14 CD8 T cells at D31 and validate the observations in the prior figures of more rapid adoption of time-dependent changes in memory (i.e. conversion to central memory) (e.g. changes in clusters 6 and 8 of ***Figure 3***). The remaining genes were then evaluated for the presence of a sepsis-induced transcriptional 'scar' to delineate conserved changes as a result of the septic event. These changes constituted the second cluster and were identified by the similar transcriptional changes for D1 Sham to CLP and D31 Sham to CLP. This sepsis-induced 'scar' constituted 113 of the 269 gene changes observed (***Table 2***) and demonstrates that some of the transcriptional changes evoked early after sepsis persist. Finally, there remained a third cluster of 57 gene changes (***Table 2***) that were neither associated with time-dependent changes in CD8 T cell memory nor were they associated with the early sepsis induced changes to memory CD8 T cells. Thus, novel transcriptional changes also arise in memory CD8 T cells during the post-septic environment. Summarily, these data demonstrate that sepsis leads to lasting changes in the transcriptional landscape of memory CD8 T cells. These changes are associated with the more rapid acquisition of time-dependent changes by memory CD8 T cells in CLP hosts, a sepsis-induced transcriptional scar, and novel transcriptional changes acquired in the post-septic environment.

To address how these transcriptional changes may be the result of an altered epigenetic landscape, chromatin accessibility was assessed in Sham and CLP P14 CD8 T cells by ATAC-sequencing at D31 post-surgery (***Figure 5f***). While 1646 peaks were differentially expressed, the changes observed were predominantly more peaks (more accessibility) in CLP hosts (***Figure 5g***). Of these the majority were either within a gene body or intergenic regions assigned to the nearest a transcription start site. Significant changes in gene expression were then compared with DCAPs to establish whether there was concordance between the gene changes observed and the accessibility of the chromatin. Indeed, there were genes whose chromatin accessibility and transcription is concordant. Importantly, these concordant genes identified potentially relevant changes in CD8 T cell function (***Figure 5h and i***). Among these *P2r×7*, *Rad51*, and *Bub1b* all have prior association with CD8 T cell survival, DNA damage repair, and cell cycling (***Baek et al., 2003***; ***Borges da Silva et al., 2018***; ***Yamamoto et al.,***

Table 2. Gene clusters.

gene_id	Relative FC D32 sham vs CLP	p_value_	**Cluster #**
Cdc6	4.03064298	0.00005	Cluster 1
Tppp3	4.88825654	0.00005	Cluster 1
Neil3	3.66496647	0.00005	Cluster 1
Hist1h1e	3.76231332	0.00005	Cluster 1
Mcm10	3.47460746	0.00005	Cluster 1
Ttc8	3.38918878	0.00005	Cluster 1
Stmn1	2.06406728	0.0508	Cluster 1
Gpr34	3.41697573	0.00005	Cluster 1
Ppp2r2c	1.83454208	0.0437	Cluster 1
Kntc1	2.99415727	0.00005	Cluster 1
Bfsp1	1.60516322	0.03045	Cluster 1
Birc5	2.8137029	0.00005	Cluster 1
Ccdc136	2.28917856	0.0344	Cluster 1
Gm5124	1.60472157	0.03095	Cluster 1
Ccnb2	2.49461988	0.00005	Cluster 1
Apol7b	2.6692603	0.00005	Cluster 1
Tktl1	1.9334132	0.02895	Cluster 1
Dtl	2.59828557	0.00005	Cluster 1
Pask	2.7640812	0.00005	Cluster 1
Crip2	2.52029044	0.0004	Cluster 1
Clspn	2.45116907	0.00015	Cluster 1
Mki67	2.61164716	0.00005	Cluster 1
Fam64a	2.65731637	0.0006	Cluster 1
2810408I11Rik	1.5215239	0.06725	Cluster 1
Rad51ap1	1.63064417	0.00235	Cluster 1
Tnfsf4	2.37518519	0.0009	Cluster 1
E2f1	2.34354094	0.031	Cluster 1
Cep55	2.4930123	0.0004	Cluster 1
Morn3	2.12074329	0.00035	Cluster 1
Aurkb	2.4030389	0.00005	Cluster 1
Hist2h2bb	2.02820011	0.0464	Cluster 1
Exo1	2.36813282	0.00005	Cluster 1
Fcrlb	1.52457593	0.04225	Cluster 1
Tmem176a	1.59714799	0.0361	Cluster 1
Socs2	2.02128114	0.00155	Cluster 1
Ncapg2	1.97320931	0.00745	Cluster 1
Klra9	2.11296665	0.00005	Cluster 1
Chek1	1.59507471	0.05475	Cluster 1
Rad51	1.58587164	0.00005	Cluster 1
Dscc1	1.74867599	0.00015	Cluster 1
Bzrap1	1.61419626	0.00005	Cluster 1
Cd300e	1.519849	0.07755	Cluster 1
Gm1720	1.94574412	0.0019	Cluster 1
Brca1	1.5604888	0.05435	Cluster 1
Gm14124	1.64708499	0.03685	Cluster 1
Shcbp1	1.79205262	0.00005	Cluster 1
Nebl	1.8053468	0.04325	Cluster 1
Ckap2l	1.73019782	0.0003	Cluster 1
Cdkn2a	1.82961741	0.00085	Cluster 1
Phlda3	1.63185741	0.03825	Cluster 1
Adgre4	1.57646266	0.00005	Cluster 1
Klri2	1.56007674	0.0011	Cluster 1
Mmp25	1.54571785	0.04745	Cluster 1
Nenf	1.5307705	0.0182	Cluster 1
Igf1	–1.524316	0.01	Cluster 1
Rac3	–1.5034855	0.07065	Cluster 1
Trf	–1.6496992	0.00015	Cluster 1
Chaf1a	–1.6002474	0.0011	Cluster 1
Orc1	–1.6245667	0.04185	Cluster 1
Fignl1	–1.7257028	0.0216	Cluster 1
D430020J02Rik	–1.6263897	0.0051	Cluster 1
Cenph	–1.8078839	0.0047	Cluster 1
Blvrb	–1.8434164	0.0457	Cluster 1
Cpne7	–1.5149666	0.02655	Cluster 1
Psrc1	–1.7535019	0.00145	Cluster 1
Uhrf1	–1.5739852	0.0013	Cluster 1
Plbd1	–1.7851892	0.0021	Cluster 1
Rgs12	–1.8455643	0.01885	Cluster 1
Hpgd	–1.8522078	0.06025	Cluster 1
P2rx7	–2.0648257	0.01595	Cluster 1
Bub1b	–2.2247142	0.0223	Cluster 1
4833418N02Rik	–2.3048295	0.011	Cluster 1
Ube2c	–1.621509	0.0124	Cluster 1
Cadm1	–2.3409109	0.00015	Cluster 1
Tyrobp	–2.4355709	0.00335	Cluster 1
Jup	–2.4842838	0.0023	Cluster 1

Table 2 continued on next page

Table 2 continued

Table 2 continued on next page

Table 2 continued

gene_id	Relative FC D32 sham vs CLP	p_value_	**Cluster #**
Pyroxd2	–2.2264265	0.0282	Cluster 1
Gins1	–1.8339216	0.00005	Cluster 1
Gm4013	–2.7505116	0.01255	Cluster 1
Axl	–2.6625156	0.00005	Cluster 1
Nr6a1	–2.729109	0.00125	Cluster 1
Hspa2	–2.796573	0.00005	Cluster 1
Spry2	–2.7405966	0.00005	Cluster 1
Mpeg1	–2.8281527	0.00005	Cluster 1
Ticrr	–2.9418017	0.00005	Cluster 1
Plxdc1	–2.9468017	0.00005	Cluster 1
Ly86	–3.2898687	0.0019	Cluster 1
Cd302	–3.3417875	0.00005	Cluster 1
C6	–3.3367417	0.0003	Cluster 1
Slc37a2	–3.3489759	0.00005	Cluster 1
Gm2011	–3.4732831	0.00005	Cluster 1
H2-T3	–2.0828371	0.00935	Cluster 1
Wnt2b	–3.5079301	0.0004	Cluster 1
Clec12a	–3.0562022	0.00895	Cluster 1
Mmp17	–4.1251312	0.00005	Cluster 1
Ncaph	–4.1603359	0.0417	Cluster 1
Kcnj10	–4.2878368	0.00005	Cluster 1
Cd163	–4.2866184	0.0001	Cluster 1
Il11	–5.666901	0.0001	Cluster 1
Syk	4.80557812	0.0603	Cluster 2
9030619P08Rik	2.73623094	0.0353	Cluster 2
Prss16	2.57604894	0.00005	Cluster 2
Tcf4	2.52783097	0.0069	Cluster 2
Itgad	2.32061951	0.00005	Cluster 2
Abcc3	2.47441931	0.0143	Cluster 2
Hfe	1.91152093	0.00065	Cluster 2
Fcgr3	1.94948898	0.00005	Cluster 2
Rab3il1	2.00253853	0.00255	Cluster 2
Lrp1	2.06172226	0.06585	Cluster 2
Cd5l	1.6117422	0.0645	Cluster 2
Mir2861	1.93355795	0.0162	Cluster 2
Il18	1.64165162	0.07875	Cluster 2
Mir155hg	1.9632828	0.0003	Cluster 2
Irf4	1.83011207	0.00085	Cluster 2

Table 2 continued on next page

Table 2 continued

gene_id	Relative FC D32 sham vs CLP	p_value_	**Cluster #**
Cmklr1	1.71253206	0.00655	Cluster 2
Mt3	1.61299839	0.00005	Cluster 2
Cd163l1	1.68200967	0.0028	Cluster 2
Palm	1.69858804	0.0309	Cluster 2
Hmox1	1.8719138	0.0014	Cluster 2
Mertk	1.69725108	0.05425	Cluster 2
Esm1	1.55538421	0.08875	Cluster 2
Lrrc25	1.53588266	0.01125	Cluster 2
Lgmn	1.53366352	0.0421	Cluster 2
Mafb	1.59909428	0.00005	Cluster 2
Havcr2	1.61859719	0.00005	Cluster 2
Epb4.1l3	1.64271249	0.0257	Cluster 2
Siglece	1.58382507	0.0091	Cluster 2
Prr5	–1.5418463	0.05615	Cluster 2
Pla2g7	–1.5675528	0.00005	Cluster 2
Dusp14	–1.6724627	0.02015	Cluster 2
Tgm2	–1.6678575	0.04595	Cluster 2
Riiad1	–1.5429946	0.00005	Cluster 2
Lilrb4a	–1.6883324	0.00685	Cluster 2
Ninj2	–1.5669531	0.08315	Cluster 2
Cish	–1.6443416	0.0508	Cluster 2
Cenpe	–1.8650444	0.07995	Cluster 2
Cenpm	–1.5922104	0.00155	Cluster 2
Tpx2	–1.5558403	0.05695	Cluster 2
Oip5	–1.7861225	0.00005	Cluster 2
Cdca7	–1.5875434	0.04035	Cluster 2
Ckap2	–1.6603956	0.00425	Cluster 2
Ncapg	–1.8932803	0.019	Cluster 2
Ssc4d	–1.9973193	0.0063	Cluster 2
Stkld1	–1.8746276	0.04135	Cluster 2
Cdca8	–1.6650517	0.0087	Cluster 2
Cdc45	–1.9715619	0.00405	Cluster 2
Lrp11	–1.9542283	0.0003	Cluster 2
Mcm5	–1.965633	0.012	Cluster 2
Cks1b	–2.0197826	0.0137	Cluster 2
Apitd1	–1.614175	0.01045	Cluster 2
Spc24	–2.1192151	0.00145	Cluster 2
Serpine2	–2.0231734	0.00005	Cluster 2

Table 2 continued on next page

Table 2 continued

gene_id	Relative FC D32 sham vs CLP	p_value_	**Cluster #**
Brip1	–1.6461742	0.092	Cluster 2
Pole	–2.2240204	0.0253	Cluster 2
Lig1	–1.7583399	0.0015	Cluster 2
Cenpn	–1.7057202	0.00005	Cluster 2
Gm19434	–2.012432	0.0005	Cluster 2
Carns1	–2.0274411	0.0205	Cluster 2
Mpp2	–1.5418367	0.00775	Cluster 2
Mustn1	–2.061708	0.0017	Cluster 2
Rn45s	–2.10963	0.07705	Cluster 2
Sema6b	–2.2547383	0.0119	Cluster 2
Cfp	–2.0456935	0.0001	Cluster 2
App	–2.211262	0.00935	Cluster 2
Car9	–2.0062063	0.02255	Cluster 2
1700102P08Rik	–2.4325509	0.0268	Cluster 2
Snhg10	–2.345361	0.00015	Cluster 2
Lima1	–2.3391753	0.07585	Cluster 2
Selm	–2.0294095	0.00265	Cluster 2
Slc41a3	–2.1887998	0.0001	Cluster 2
Src	–2.6392902	0.00015	Cluster 2
Miat	–2.5487856	0.0109	Cluster 2
Cd79a	–2.5900501	0.00055	Cluster 2
Plxnb2	–2.9874612	0.00005	Cluster 2
Pla2g2d	–1.529167	0.0268	Cluster 2
Lyz2	–2.9362402	0.04775	Cluster 2
Cdk3-ps	–3.0692156	0.00265	Cluster 2
Mir6236	–2.5029162	0.0004	Cluster 2
Smagp	–1.9662967	0.00005	Cluster 2
AF251705	–2.8636993	0.0226	Cluster 2
Gfra2	–2.8780666	0.00005	Cluster 2
Tmem91	–3.2171875	0.00005	Cluster 2
Pld4	–1.5079912	0.02785	Cluster 2
Itgb5	–1.6713455	0.00225	Cluster 2
Treml4	–3.2826024	0.0001	Cluster 2
Cd14	–2.7112347	0.00005	Cluster 2
Marcks	–3.1963602	0.00005	Cluster 2
Cmbl	–2.6693158	0.00005	Cluster 2
Klra3	–2.5417462	0.03455	Cluster 2
Ctsh	–3.5891694	0.00565	Cluster 2

Table 2 continued on next page

Table 2 continued

gene_id	Relative FC D32 sham vs CLP	p_value_	**Cluster #**
Klra8	–3.3087585	0.0001	Cluster 2
Cd81	–3.3276415	0.00005	Cluster 2
C1qb	–3.7316146	0.00005	Cluster 2
Aif1	–3.2695906	0.01525	Cluster 2
Bank1	–3.0876517	0.002	Cluster 2
C1qc	–3.0727492	0.0001	Cluster 2
Apoe	–3.5282676	0.00005	Cluster 2
Clec4a3	–2.9215824	0.00015	Cluster 2
Tgfbi	–3.5641054	0.00005	Cluster 2
Mrc1	–3.6479097	0.03025	Cluster 2
Sirpa	–4.0829446	0.00005	Cluster 2
Clec1b	–1.7537681	0.0004	Cluster 2
Klra14-ps	–3.8984753	0.00005	Cluster 2
Ccr3	–2.5323907	0.06515	Cluster 2
C1qa	–3.5880749	0.00005	Cluster 2
Vcam1	–3.6726209	0.0011	Cluster 2
Tbxas1	–4.4023688	0.00005	Cluster 2
Csf1r	–4.0805398	0.00005	Cluster 2
Fcna	–3.3668046	0.00005	Cluster 2
Adgre1	–3.7926073	0.00005	Cluster 2
Adamdec1	–4.9789792	0.00005	Cluster 2
Tnfrsf8	–2.2700751	0.0008	Cluster 2
Aldh2	2.4260512	0.00025	Cluster 3
Slc40a1	2.40044187	0.0057	Cluster 3
Zfp385a	2.16534965	0.06435	Cluster 3
Spag5	1.88610893	0.00005	Cluster 3
Nusap1	1.84390075	0.09965	Cluster 3
B9d1	1.78604818	0.0031	Cluster 3
Top2a	1.74249558	0.0044	Cluster 3
Alox5ap	1.64982614	0.09075	Cluster 3
Sgol2a	1.61420186	0.05365	Cluster 3
Cdk1	1.59276453	0.0489	Cluster 3
Pla2g4b	1.58954405	0.04465	Cluster 3
Fam174b	1.54600394	0.00895	Cluster 3
Spc25	1.51665085	0.0962	Cluster 3
Ppp1r13l	–1.5091602	0.0399	Cluster 3
Neto2	–1.5160875	0.0106	Cluster 3
Eif3j2	–1.5188243	0.03625	Cluster 3

Table 2 continued on next page

Table 2 continued

gene_id	Relative FC D32 sham vs CLP	p_value_	**Cluster #**
Gm28042	–1.5257346	0.02945	Cluster 3
Gm4532	–1.5651414	0.05395	Cluster 3
Sowahc	–1.5972355	0.09105	Cluster 3
Tnfrsf21	–1.6215854	0.04005	Cluster 3
Gm3435	–1.6321142	0.01435	Cluster 3
Zfp112	–1.6371301	0.04985	Cluster 3
Nr1h3	–1.6602966	0.07725	Cluster 3
2810468N07Rik	–1.6797191	0.0173	Cluster 3
Hck	–1.6894024	0.04875	Cluster 3
Pth1r	–1.7203976	0.06865	Cluster 3
Tagln3	–1.7598763	0.05825	Cluster 3
Hist1h4d	–1.7606181	0.0688	Cluster 3
Tubb3	–1.803737	0.00005	Cluster 3
Klre1	–1.8122236	0.02795	Cluster 3
Spi1	–1.8248628	0.0498	Cluster 3
Fcgr4	–1.8961012	0.01005	Cluster 3
Mrgpre	–1.9259777	0.00455	Cluster 3
Chrne	–1.9429018	0.03985	Cluster 3
Tctex1d2	–1.9516374	0.00005	Cluster 3
Sdc3	–1.9572554	0.0026	Cluster 3
Tlr7	–1.9874423	0.0019	Cluster 3
Slc11a1	–2.0856253	0.001	Cluster 3
Gzma	–2.102273	0.00005	Cluster 3
Cpsf4l	–2.1529279	0.0146	Cluster 3
Clec4a1	–2.2106337	0.0132	Cluster 3
Fcer1g	–2.2631622	0.0002	Cluster 3
Ncf2	–2.2765987	0.00205	Cluster 3
Slpi	–2.2838533	0.00005	Cluster 3
Cd244	–2.4303599	0.0011	Cluster 3
Ptgs1	–2.5181601	0.0003	Cluster 3
Cybb	–2.7556258	0.0001	Cluster 3
Matk	–3.0595087	0.00005	Cluster 3
Ifitm2	–3.1387932	0.01575	Cluster 3
Cdc20b	–3.2338662	0.00705	Cluster 3
Msc	–3.4433671	0.01	Cluster 3
Clec4n	–3.4851723	0.00015	Cluster 3
Rgl1	–3.5597601	0.0001	Cluster 3
Spic	–3.6767727	0.00005	Cluster 3

Table 2 continued on next page

Table 2 continued

gene_id	Relative FC D32 sham vs CLP	p_value_	**Cluster #**
Hebp1	–3.7616875	0.00025	Cluster 3
Hist1h3e	–4.1043962	0.04245	Cluster 3
Lrg1	–5.383073	0.0033	Cluster 3

1996). Thus, the increase in the expression of these genes in CLP P14 CD8 T cells likely reflects the numerical recovery after sepsis and general shift toward T_{CM}. Conversely, the increased expression of *Cish* and decreased expression of *Itgad*, which inhibit TCR functional avidity (***Palmer et al., 2015***) and promote cell adhesion (***Siegers et al., 2017***), respectively, demonstrate the function of surviving CD8 T cells may be compromised or altered. This is particularly interesting given that the TCR is itself fixed in these populations thus the variations are not attributable to changes in the composition of the TCR repertoire, a finding that would not be obvious in a polyclonal TCR population. To relate these findings back to the phenotypic differences observed previously, the chromatin accessibility within the *Sell* locus (which encodes CD62L) was compared between P14 CD8 T cells from Sham and CLP hosts (***Figure 5i***). Critically, there was increased accessibility in the CD62L locus of P14 CD8 T cells from CLP hosts, relative to Sham (indicated in the boxed regions). Thus, the increased accessibility at the *Sell* locus corresponds to increased transcription at that locus (***Figure 5j***) and a subsequent increase in the expression of CD62L (***Figure 4***). Importantly, the transcription of the additional phenotypic distinctions observed in ***Figure 3*** largely conformed wherein there was decreased expression of *Cx3cr1* and *Klrg1* (***Figure 5j***), though no change in expression was observed for other markers such *Cxcr3* and *Il7r*. Thus, sepsis leads to lasting changes in chromatin accessibility, some of which are concordant with gene expression. The resulting transcriptional changes are likely to reflect functional outcomes consistent with the composition of the memory CD8 T cell population.

To interrogate putative functional impairments, gene-set enrichment analysis (GSEA) was performed to compare Sham and CLP memory P14 CD8 T cells at D31 post-surgery. When evaluating the top five positively enriched KEGG pathways in CLP P14 CD8 T cells, there was an obvious trend toward cell cycling (***Figure 6a***). Specifically, the pathways included: KEGG_Ribosome,

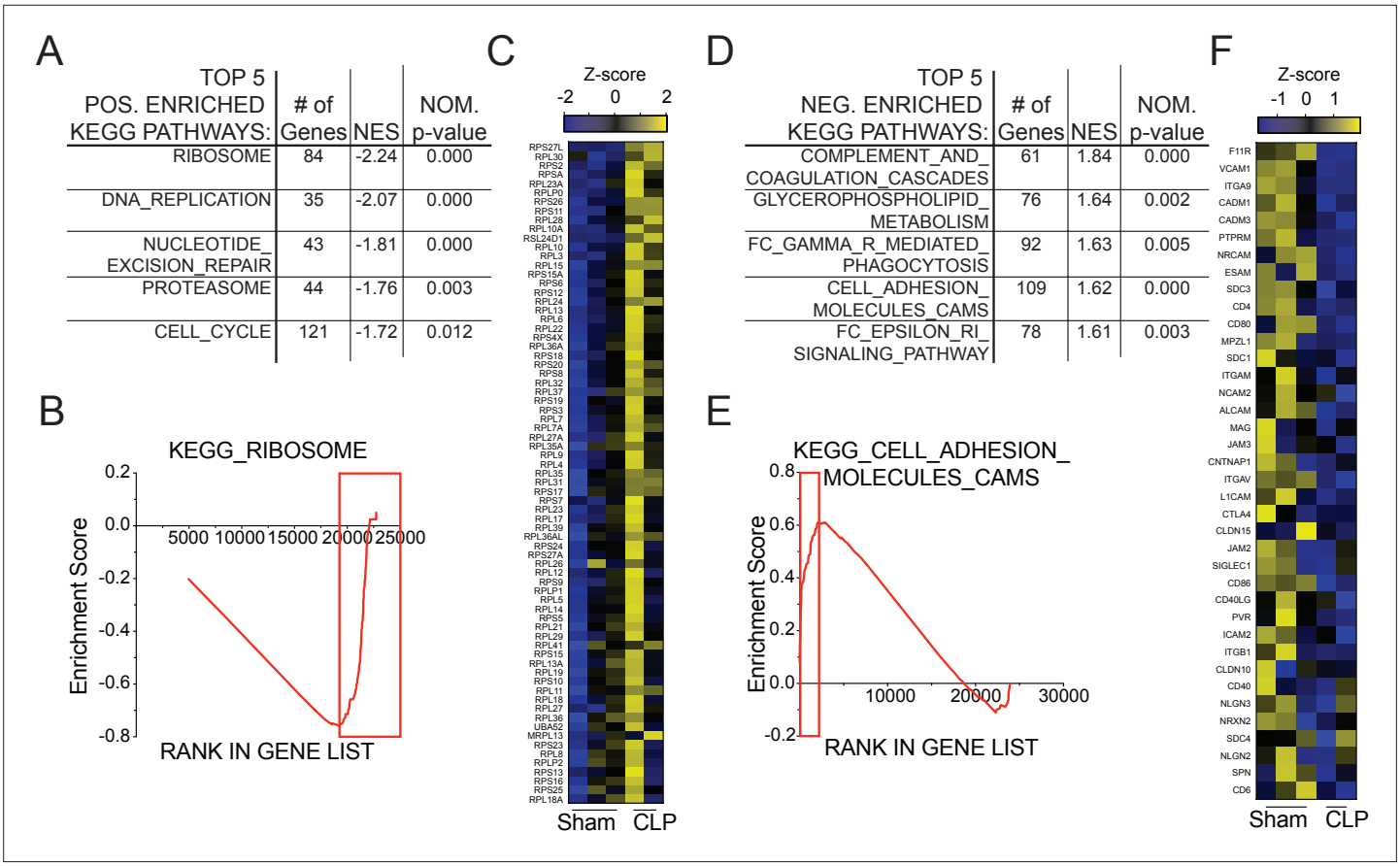

Figure 6. Gene set enrichment analysis (GSEA) reveals long-term sepsis-induced differences in molecular pathways of pre-existing memory CD8 T cells. Top 5 KEGG pathways positively- (**A**) and negatively- (**D**) enriched in CLP hosts. Enrichment scores for Ribosomal- (**B**) and Adhesion- (**E**) associated genes. Red box indicates leading edge of enriched region; genes enriched in CLP - box to right, genes enriched in Sham – box to left. Gene expression heatmap of core enriched genes for Ribosomal (**C**) and Adhesion (**F**) associated genes.

The online version of this article includes the following figure supplement(s) for figure 6:

Source data 1. Source data for ***Figure 6***.

Figure supplement 1. Gene set enrichment analysis (GSEA) reinforces that sepsis promotes a shift to T_{CM} at transcriptional level.

Figure supplement 1—source data 1. Source data for ***Figure 6—figure supplement 1A-D***.

_DNA_Replication, _Nucleotide_Excision_Repair, _Proteasome, and _Cell_Cycle. In conjunction with the concordant gene analysis (***Figure 5g***), this information further supports the notion that the numerical recovery after sepsis alters the composition of memory CD8 T cells through proliferation. A critical example of this is the substantial enrichment of ribosomal proteins (***Figure 6b and c***), putatively necessary for increased translational output during proliferation. Conversely, several pathways were also negatively enriched in CLP P14 CD8 T cells (positively enriched in Sham), including: KEGG_Complement_And_Coagulation_Cascades, _Glycerophopholipid_Metabolism, _FC_Gamma_R_Mediated_Phagocytosis, _Cell_Adhesion_Molecules_CAMS, and _FC_Epsilon_RI_Signaling_Pathway (***Figure 6d***). The primary underlying connection between the first two and last two of these appears to be linked to integrin expression and cell adhesion, while the change in glycerophospholipid metabolism may suggest sepsis-induced metabolic alterations. Given that integrin expression was also identified among the concordant genes in ***Figure 5g***, gene enrichment in KEGG_Cell_Adhesion_Molecules_CAMS was evaluated and reduced expression of additional integrins was observed (***Figure 6e and f***). Given the critical nature of integrins in TCR function, including TCR-dependent function and immunologic synapse formation, these data suggest that sepsis alters the intrinsic capacity of pre-existing memory CD8 T cells to recognize cognate antigen. Further, when we compared the transcriptional changes between Sham D31 and CLP D31 with the published data

set KAECH_DAY15_EFF_VS_MEMORY_CD8_TCELL we observed that P14s from Sham hosts were biased toward effector CD8 T cells while the P14s from CLP hosts were biased toward memory CD8 T cells, mirroring the shift from effector to central CD8 T cell memory (***Figure 6—figure supplement 1***). This reinforces our observation of sepsis accelerating the adoption of time-dependent changes in the composition of the memory CD8 T cell pool.

Sepsis-induced changes in pre-existing memory CD8 T cell composition impact cell function and capacity to control infection

To address the putative functional alterations resulting from sepsis-induced changes in the memory CD8 T cell pool, the capacity of memory P14 CD8 T cells to undergo TCR-dependent adhesion and immunologic synapse formation >30 days after either Sham or CLP surgery was assessed (***Figure 7—figure supplement 1a***). Notably, impairment in adherence capacity was observed in P14 CD8 T cells from CLP hosts under limiting stimulation conditions (low αCD3 concentration; ***Figure 7—figure supplement 1b, c***); however, when stimulation was not limiting (high αCD3 concentration) Sham and CLP P14 CD8 T cells were equally capable of undergoing TCR-dependent adhesion. The TCR-induced signaling complex was then assessed via TIRF microscopy, under equivalent adherence conditions (high aCD3 concentration), to assess clustering of AKT, a surrogate of the TCR-induced signaling complex. Importantly, despite equal capability to adhere there remained a deficit in the ability to cluster AKT at the cell membrane following TCR stimulation (***Figure 7—figure supplement 1d, e***). Thus, sepsis leads to lasting changes in TCR based function of pre-existing memory CD8 T cells.

To address how these changes in signaling capability may influence cytokine production Sham and CLP splenocytes were disparately CFSE labeled >30 days post-surgery and then mixed for in vitro peptide stimulation (***Figure 7a***). Given that APCs from Sham and CLP hosts are shared in this scenario, discrepancies in function are not the result of differences in antigen display. Intriguingly, there was no deficiency in capacity to produce IFNγ, yet P14 CD8 T cells from CLP hosts actually had a higher capacity to produce IL-2 (***Figure 7b–d***). Importantly, similar results were observed after peptide (GP33) stimulation of the endogenous virus-specific memory CD8 T cell population (***Figure 7—figure supplement 2***). Indeed, this finding conforms precisely with the shift toward T_{CM} in CLP hosts since T_{CM} have greater capacity to produce IL-2 than T_{EM}. These data also suggest that changes in the composition of pre-existing memory CD8 cells may dominantly impact the function of the population as a whole.

With the relationship between the composition of the memory CD8 T cell pool and their capacity to promote effector function in mind, we next interrogated the ability of these memory CD8 T cells to control infection. Nolz et al. previously demonstrated that T_{EM} more effectively control virulent *Listeria monocytogenes* (*L.m.*) infection compared to T_{CM} (***Nolz and Harty, 2011***), likely due to localization of cells in either non-lymphoid tissues (critically the liver) or lymphoid tissues, respectively. Therefore, to address whether the shift toward T_{CM} in the CLP host impaired the subsequent capacity to control *L.m.*, P14 CD8 T cells were enriched from either Sham or CLP hosts > 30 days post-surgery then transferred to naïve recipients. Transfer of these cells into naive recipients alleviates potential environmental deficits imposed by sepsis and allows for direct assessment of the capacity of the memory CD8 T cells to control infection. Additionally, the use of naive recipients alleviates confounding variables such as bystander responses (***Ehl et al., 1997***; ***Lertmemongkolchai et al., 2001***). One day after transfer, mice that received either no cell transfer, P14 CD8 T cells from Sham mice, or P14 CD8 T cells from CLP were challenged with virulent *L.m.* expressing GP_{33}. *L.m.* challenge occurred 1 day after cell transfer to allow time for the cells to distribute and localize to their respective niches. GP_{33} expression by *L.m.* enables the memory P14 CD8 T cells to mediate antigen-specific control. Colony-forming units (CFU) in both the liver and spleen were assessed 5 days post-infection (***Figure 7e***). Recipients that received memory P14 CD8 T cells from either Sham or CLP hosts more robustly controlled *L.m.* infection than the naive hosts that did not receive any memory CD8 T cells (***Figure 7f and g***). However, memory P14 CD8 T cells from Sham recipients were significantly better at controlling *L.m.* than those from CLP recipients; 77- and 20-fold differences control in the liver and spleen, respectively (***Figure 7f and g***). This improved control by memory P14 CD8 T cells from Sham hosts demonstrates the higher capacity of T_{EM} to control *L.m.* infection. Thus, our data cumulatively demonstrate how sepsis-induced changes in the composition of the pre-existing memory CD8 T cells alters the functional capability of the memory CD8 T cell population as a whole, thereby altering the host response to infection.

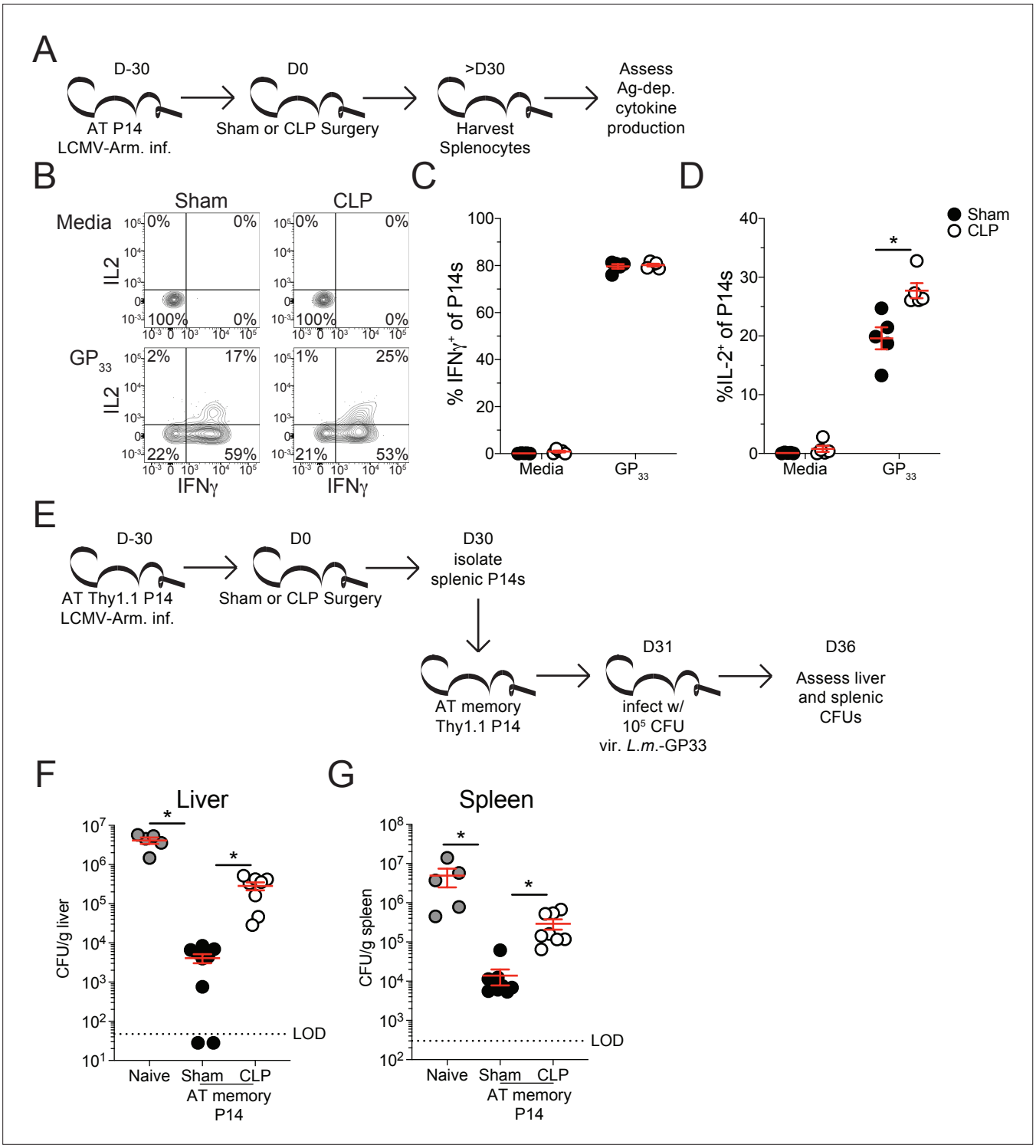

Figure 7. Sepsis leads to lasting changes in pre-existing memory CD8 T cell function and *Listeria* control. (**A**) Experimental Design: Antigen-experienced P14 chimeric mice were generated by adoptive transfer of 5 × 10^3 naive Thy1.1$^+$ TCR-transgenic P14 CD8 T cells to Thy1.2$^+$ C57Bl/6 mice that were subsequently infected with LCMV-Arm. Mice underwent Sham or CLP surgery 30 days after infection. Splenocytes from Sham and CLP mice were isolated 30 days after surgery and disparately labeled with CFSE, mixed, and then placed in media alone (i.e. unstimulated) or stimulated GP_{33} peptide. Representative profiles (**B**) and quantification of the frequency of IFN γ - (**C**) and IL-2- (**D**) producing P14s stimulated with either media control or GP_{33}. Data are representative of two independent experiments with 5 mice per group. (**E**) Experimental Design: Antigen-experienced P14 chimeric mice were generated by adoptive transfer of 5 × 10^3 naive Thy1.1$^+$ TCR-transgenic P14 CD8 T cells to Thy1.2$^+$ C57Bl/6 mice that were subsequently infected with LCMV-Arm. Mice underwent Sham or CLP surgery 30 days after infection. Splenic P14 CD8 T cells were enriched from Sham and CLP mice

Figure 7 continued on next page

Figure 7 continued

30 days after surgery and then transferred into naïve mice. Mice that received either Sham or CLP P14 CD8 T cells, or did not receive any cell transfer (i.e. naïve) were then infected with 10^5 CFU of *Listeria monocytogenes* expressing GP_{33} (*L.m.*-GP_{33}) 1 day later. CFU of *L.m.*-GP_{33} per gram of liver (**F**) and spleen (**G**) was assessed 5 days after infection. Data are cumulative of two independent experiments with 5–9 mice per group. *=$p < 0.05$. Error bars indicate standard error of the mean.

The online version of this article includes the following figure supplement(s) for figure 7:

Source data 1. Source data for ***Figure 7C and D***.

Source data 2. Source data for ***Figure 7F and G***.

Figure supplement 1. Sepsis leads to lasting deficit in pre-existing memory CD8 T cell TCR-dependent adhesion and immunologic synapse formation.

Figure supplement 1—source data 1. Source data for ***Figure 7—figure supplement 1c***.

Figure supplement 1—source data 2. Source data for ***Figure 7—figure supplement 1e***.

Figure supplement 2. Sepsis leads to lasting changes in pre-existing polyclonal memory CD8 T cell function.

Figure supplement 2—source data 1. Source data for ***Figure 7—figure supplement 1***.

Discussion

In the present study, we demonstrate that sepsis leads to a lasting change in the composition of the memory CD8 T cell compartment in the sepsis survivors. This occurs as a result of proliferation in the lymphopenic environment that occurs after sepsis, seen in both patients and mice, wherein T_{CM} have higher proliferative capacity than T_{EM}. This biasing toward T_{CM} alters the localization of memory CD8 T cells. Further, the memory CD8 T cell pool has an altered transcriptional landscape and chromatin accessibility, which is associated both with the transition toward T_{CM} and functional alterations. The culmination of these sepsis-induced changes alters the function of the memory CD8 T cells and reduces their capacity to control virulent *L.m.* infection.

There are several important implications of the present study, and the biasing toward T_{CM}, that are relevant to our understanding of the immunoparalysis state. Among these is the relationship to tissue resident memory CD8 T cells (T_{RM}), which provide sensing and alarm function at sites of prior infection (***Masopust et al., 2001***; ***Schenkel et al., 2013***). The present study focuses on the influence of sepsis on circulating T_{EM} and T_{CM} CD8 T cells; however, the substantial population of T_{RM} throughout the body may be an interesting source of future interrogation. Danahy et al. previously demonstrated that T_{RM} were not susceptible to sepsis-induced lymphopenia, due to their exclusion from the vasculature (***Danahy et al., 2017***). In the present study, recovery in cellularity was observed with time after sepsis, but the biasing toward T_{CM} may pose a particular problem for T_{RM}. Specifically, Slütter et al. demonstrated that lung T_{RM} are seeded from circulating T_{EM} (***Slütter et al., 2017***). Thus, the challenge to the T_{RM} may be twofold: (1) the reduced seeding of cells during the lymphopenic state and (2) reduced T_{EM} pool from which to seed the T_{RM}. This reduction may culminate in a more rapid waning of lung T_{RM} and reinforce susceptibility to previously encountered infections. Moreover, the detrimental effects of sepsis on memory CD8 T cells may also be relevant to other major inflammatory events and poorly controlled infections (e.g. SARS-CoV-2) and should be considerations in the long-term consequences for similarly impacted individuals (***Li et al., 2020***; ***Sariol and Perlman, 2020***).

While the immunoparalysis state is often viewed directly through the lens of the detriments that may arise, it is also relevant to consider other means by which the host immune response may be shaped. The loss of T_{EM} here demonstrates their critical role in fighting some infections (i.e. *L.m.*) (***Nolz and Harty, 2011***); however, T_{CM} are also a potent population that can critically mediate control in other infection scenarios. Thus, infections for which T_{CM} can provide critical control may be unimpaired or even enhanced in the post-septic environment. This is potentially complicated by intrinsic deficits that may be present in the memory cells, as observed in our GSEA analysis and by CD8 T cell extrinsic impairments. Therefore, future studies should consider additional interrogation of mechanisms by which the immune system is altered beyond detrimental aspects. Additionally, while our interrogation focused on a shift of pre-existing memory CD8 T cells toward a central memory phenotype, it remains possible that other T cell populations (e.g. different antigen specificities) may bias toward effector memory. This may be particularly relevant to memory T cell populations whose TCR has some low degree of cross reactivity with antigens present on microbes released during the septic event. These

considerations may be important for future therapeutic interrogation in the specific targeting of the appropriate deficits.

Additionally, it is relevant to consider that proliferation, as demarcated by Ki67, was also observed in naïve CD8 T cells of septic patients. While not the focus of the present study this is also observed in our mouse model. The proliferation by naïve CD8 T cells in septic hosts suggests that CD8 T cells are proliferating in response to the lymphopenic environment. Indeed, naive cells undergo antigen-independent proliferation in other lymphopenic environments, such *as Rag*$^{-/-}$ or irradiated hosts, wherein they adopt conventional markers of antigen experience along with some effector functionality (***Cheung et al., 2009***; ***Pribikova et al., 2018***; ***Unsinger et al., 2009***; ***White et al., 2017***). Thus, it may be relevant to consider how the proliferation of these cells also alter the composition of the memory CD8 T cell compartment and shapes host response to subsequent infection for which they may be specific.

Our novel characterization of how numeric recovery in the lymphopenic environment alters the composition of the memory CD8 T cell compartment demonstrates how sepsis can lead to lasting changes in host immunity. However, the implications of these changes may extend beyond the enhanced susceptibility to infection described here to potentially reframe our understanding of the immunoparalysis state. Future interrogation of these lasting effects will likely be required to best address the deficits that arise in the immunoparalysis state. Further understanding how sepsis shapes both naive and memory T cells may also alternately produce therapeutic interventions to benefit other diseases. One such example may be in the promotion of T_{CM} over T_{EM}, or vice versa, for specific vaccination strategies. Such outcomes and lines of investigation would be highly instructive for understanding how prior immune history shapes subsequent host immune responses.

Materials and methods

Key resources table

Reagent type (species) or resource	Designation	Source or reference	Identifiers	Additional information
Strain, strain background (*Mus musculus*)	C57BL6/J	Jackson Laboratory	Stock No: 000664 (RRID:IMSR_JAX:000664)	
Strain, strain background (*Mus musculus*)	B6.PL(84NS)/Cy	Jackson Laboratory	Stock No: 000983 (RRID:IMSR_JAX:000406)	C57BL6/J Thy1.1
Strain, strain background (*Mus musculus*)	B6.Cg-Tcratm1Mom Tg(TcrLCMV)327Sdz (P14)	Jackson Laboratory	Stock No: 37394-JAX (RRID:IMSR_TAC:4138)	
Strain, strain background (*Mus musculus*)	Thy1.1/1.1- B6.Cg-Tcratm1Mom Tg(TcrLCMV)327Sdz	This paper	Thy1.1/1.1 P14	Can be acquired through lab contact or breeding of above commercially available strains
Strain, strain background (Lymphocytic choriomeningitis virus)	Lymphocytic choriomeningitis virus Armstrong strain (LCMV-Arm)	Armstrong, C. and Lillie, R.D. Experimental lymphocytic choriomeningitis of monkeys and mice produced by a virus encountered in studies of the 1933 St Louis encephalitis epidemic. *Public Health Reports* 49, 1019–1027 (1934)	LCMV-Arm	Can be acquired through lab contact.
Strain, strain background (virulent Listeria monocytogenes)	Virulent recombinant *Listeria monocytogenes* expressing GP33-41 (XFL203 *L.m.*-GP33)	Shen et al. Recombinant Listeria monocytogenes as a live vaccine vehicle for the induction of protective anti-viral cell-mediated immunity. *PNAS* 92(9) 3987–3991 (1995)	*L.m.*-GP33	Can be acquired through lab contact.
Peptide, recombinant protein	GP33-44	AnaSpec	Catalog #: AS-61296	
Antibody	CD8a (Rat monoclonal)	Biolegend	5H10-1 (RRID:AB_312762)	FACs (1:400)
Antibody	CD11a (Rat monoclonal)	Biolegend	M17/4 (RRID:AB_312776)	FACs (1:300)
Antibody	Thy1.1 (Mouse monoclonal)	eBioscience	HIS51 (RRID:AB_1257173)	FACs (1:1000)
Antibody	KLRG1 (Mouse monoclonal)	eBioscience	2F1 (RRID:AB_540279)	FACs (1:100)

Continued on next page

Continued

Reagent type (species) or resource	Designation	Source or reference	Identifiers	Additional information
Antibody	CD127 (Rat monoclonal)	eBioscience	eBioSB/199	FACs (1:100)
Antibody	CD62L (Rat monoclonal)	Biolegend	MEL-14 (RRID:AB_1853103)	FACs (1:100)
Antibody	CX3CR1 (Mouse monoclonal)	eBioscience	SA011F11 (RRID:AB_2565701)	FACs (1:100)
Antibody	CXCR3 (Armenian Hamster monoclonal)	eBioscience	CXCR3-173 (RRID:AB_1210593)	FACs (1:100)
Antibody	CD27 (Armenian Hamster monoclonal)	eBioscience	LG.7F9	FACs (1:100)
Antibody	CD69 (Hamster monoclonal)	Biolegend	H1.2F3 (RRID:AB_1853105)	FACs (1:100)
Antibody	CD103 (Hamster monoclonal)	Biolegend	2E7 (RRID:AB_469040)	FACs (1:100)
Antibody	CD25 (Mouse monoclonal)	Biolegend	PC61.5	FACs (1:100)
Antibody	CD122 (Rat monoclonal)	Biolegend	TM-b1	FACs (1:100)
Antibody	IFNγ (Rat monoclonal)	eBioscience	XMG1.2 (RRID:AB_465410)	FACs (1:100)
Antibody	IL-2 (Rat monoclonal)	Biolegend	JES6-5H4 (RRID:AB_315298)	FACs (1:100)
Antibody	Ki67 (Mouse monoclonal)	BD Pharmingen	B56 (RRID:AB_2858243)	FACs (1:100)
Antibody	BrdU (Mouse monoclonal)	Biolegend	Bu20a (RRID:AB_1595472)	FACs (1:100)
Antibody	CD45RA (Mouse monoclonal)	Tonbo	HI100	FACs (1:100)
Antibody	CD45RO (Mouse monoclonal)	Tonbo	UCHL1	FACs (1:100)
Antibody	CD3 (Mouse monoclonal)	Biolegend	HIT3a	FACs (1:100)
Antibody	CD8a (Mouse monoclonal)	Biolegend	HIT8a	FACs (1:100)
Antibody	CCR7 (Mouse monoclonal)	Biolegend	G043H7	FACs (1:100)
Antibody	CD3 (Mouse monoclonal)	Biolegend	OKT3	Plate coating (0–10 µg)
Antibody	CD8a (Rat monoclonal)	Biolegend	53–6.7	FACs (1:100)
Antibody	AKT (rabbit monoclonal)	Cell Signaling Technology	11E7	TIRF microscopy (1:20)
Antibody	Anti-rabbit IgG (donkey monoclonal)	Biolegend	Poly4064	TIRF microscopy (1:100)
Commercial assay or kit	Foxp3/ Transcription Factor Staining Buffer Set	Invitrogen	00-5523-00	
Software, algorithm	GraphPad Prism	GraphPad Prism 8	Version 8.4.2 (464) (RRID:SCR_002798)	

Mice

Inbred C57Bl/6 (B6, Thy1.2) and TCR-transgenic (TCR-Tg) P14 (Thy1.1) mice were purchased from the National Cancer Institute (Frederick, MD) and maintained in the animal facilities at the University of Iowa at the appropriate biosafety level according to the University of Iowa Animal Care and Use Committee and National Institutes of Health guidelines. Male and female mice > 6 weeks of age were used for experiments; no discernable differences were observed based on sex of the animals.

Generation of antigen-experienced CD8 T cells; P14 chimeras

To generate antigen-experienced CD8 T cells 5×10^3 naïve P14 TCR-Tg CD8 T cells were adoptively transferred into recipient mice, followed a day later by infection with 10^5 plaque forming units (PFU) of Lymphocytic Choriomeningitis Virus-Armstrong (LCMV-Arm) by intraperitoneal (i.p.) injection.

Institutional setting and IRB approval

Patients were recruited at the University of Iowa Hospitals and Clinics, an 811-bed academic tertiary care center. Blood sample acquisition, patient data collection, and analysis were approved by the University of Iowa Institutional Review Board (ID #201804822). Informed consent was obtained from patients or their legally authorized representatives.

Sepsis patient selection and data collection

Subjects 18 years of age or older meeting Sepsis-3 criteria for sepsis or septic shock (***Singer et al., 2016***) secondary to intra-abdominal infection, soft tissue infection, bloodstream infection, or pneumonia were enrolled. Exclusion criteria were infection requiring antibiotics in the past month, hospitalization for infection in the past year, and chemotherapy or radiation within the past year were excluded. Demographics and baseline characteristics including age, gender, race, APACHE II score, SOFA score, and presence of septic shock were collected. EDTA-treated blood samples were collected within 24 hr of presentation.

Healthy control patient selection and data collection

Healthy volunteers 25–80 years of age were recruited from University of Iowa faculty, staff, and graduate/professional students. Exclusion criteria were signs or symptoms of active infections, infection requiring antibiotics within the past month, infection requiring hospitalization in the past year, and chemotherapy or radiation in the past year. Demographic data including age, gender, and race were collected. EDTA-treated blood samples were collected at an initial visit to our research clinic.

Human cell isolation and cryopreservation

Human cell isolation was adjusted from the previously described methodology (***Lauer et al., 2017***). Briefly, whole blood was centrifuged, and plasma removed. ACK red blood cell lysis buffer was then added to the cell pellet and rested for 5 min at room temperature. Cells were again centrifuged, and supernatant was removed. Lysis and centrifugation was repeated one to two additional times. Cells were then washed with PBS three times before being counted and resuspended in cell freeze media (90%FCS [Hyclone] 10%DMSO [Fischer Scientific]). Cells were then stored at –80 °C until use. When used in vitro, PBL were rapidly thawed and placed into warmed complete media. Cells were then washed three times with warmed media and aggregates filtered prior to use.

Cell isolation

Peripheral blood was collected by submandibular cheek bleeds to obtain PBL. Single-cell suspensions from spleen, liver, and lymph nodes were generated after mashing tissue through a 70 µm cell strainer without enzymatic digestion. Liver cells were subsequently run on a 35 % Percoll gradient. ACK lysis buffer was used for red blood cell lysis of PBL, spleen, and liver samples.

Flow cytometry, peptides, and cytokine detection

Flow cytometry data were acquired on a FACSCanto or LSRII (BD Biosciences, San Diego, CA) and analyzed with FlowJo software (Tree Star, Ashland, OR). FlowJo Software was also used for FlowSOM and tSNE analysis. To determine expression of cell surface proteins, mAb were incubated at 4 °C for 20–30 min and cells were fixed using Cytofix/Cytoperm Solution (BD Biosciences) and, in some instances, followed by incubation with mAb for an additional 20–30 min to detect intracellular proteins. The following mAb clones were used to stain murine samples: CD8a (53–6.7; eBioscience), CD11a (M17/4; Biolegend), Thy1.1 (HIS51; eBioscience), KLRG1 (2F1; Biolegend), CD127 (eBioSB/199; eBioscience), CD62L (MEL-14; eBioscience), CX3CR1 (SA011F11; Biolegend), CXCR3 (CXCR3-173; Biolegend), CD27 (LG.7F9; eBioscience), CD69 (H1.2F3; Biolegend), CD103 (2E7; eBioscience), CD25 (PC61.5; eBioscience), CD122 (TM-b1; eBioscience), IFNγ (XMG1.2; eBioscience), IL-2 (JES6-5H4; eBioscience), Ki67 (B56; eBioscience) and BrdU (Bu20a; eBioscience). The following mAb clones were

used staining of patient samples: CD45RA (HI100; Tonbo), CD45RO (UCHL1; Tonbo), CD3 (HIT3a; Biolegend), CD8a (HIT8a; Biolegend), and CCR7 (G043H7; Biolegend). Overnight fixation with FoxP3 fixation/permeabilization (eBioscience) buffer was used to stain Ki67 and BrdU. For BrdU staining, following fixation/ permeabilization cells were treated with DNAse I for 1 hr at 37 °C, then stained for intracellular BrdU.

Cecal ligation and puncture (CLP) model of sepsis induction

Mice were anesthetized with ketamine/xylazine (University of Iowa, Office of Animal Resources), the abdomen was shaved and disinfected with Betadine (Purdue Products), and a midline incision was made (***Sjaastad et al., 2020a***). The distal third of the cecum was ligated with Perma-Hand Silk (Ethicon), punctured once (for CLP_{20}) or twice (for CLP_{50}) using a 25-gauge needle, and a small amount of fecal matter extruded out of each puncture. The cecum was then returned to abdomen, the peritoneum was closed with 641 G Perma-Hand Silk (Ethicon), and skin sealed using surgical Vetbond (3 M). Following surgery, 1 mL PBS was administered s.c. to provide post-surgery fluid resuscitation. Bupivacaine (Hospira) was administered at the incision site, and flunixin meglumine (Phoenix) was administered for postoperative analgesia. Sham mice underwent identical surgery excluding cecal ligation and puncture.

Normalized assessment of lymphopenia (Figure 2C)

Due to large differences in the number of naïve to antigen-experienced endogenous cells to antigen-experienced P14 CD8 T cells in order to compare the relative degree of lymphopenia the data for each population was normalized. Data are normalized as: % survival = (1-((# of [Naive, Endo, or P14] CD8 T cells in the PBL of the same mouse prior to surgery) - (# of [Naive, Endo, or P14] CD8 T cells in the PBL of a mouse at D2 post-surgery)) / (# of [Naive, Endo, or P14] CD8 T cells in the PBL of the same mouse prior to surgery)) * 100.

BrdU administration

BrdU was administered by a single i.p. injection (2 mg/mouse) followed by ad libitum consumption in the drinking water (0.8 mg/mL) for 7 days.

RNA-seq and gene set enrichment analysis

Total RNA was extracted from P14 (Thy1.1^{+}CD8a^{lo}CD11a^{hi}) CD8 T cells sorted 1 day post-Sham or CLP and 31 days post-Sham or CLP, 2–3 biological replicates were obtained for each group. Libraries were sequenced on Illumina's HiSeq2000 in single-end mode with the read length of 50 nucleotides. The RNA-seq data are deposited at the GEO (GSE174358) under the SuperSeries of GSE174359. RNA-seq was performed as previously described (***Shan et al., 2017***). The sequencing quality of RNA-seq libraries was assessed by FastQC v0.11.4 (http://www.bioinformatics.babraham.ac.uk/projects/fastqc/). Adaptor sequences were removed through Cutadapt. The reads were mapped to mouse genome mm9 using Tophat (v2.1.0) (***Trapnell et al., 2009***). Mapped reads were then processed by Cuffdiff (v2.2.1) to estimate the expression level of all genes and identify differentially expressed genes. The expression level of a gene was expressed as a gene-level Fragments Per Kilobase of transcripts per Million mapped reads (FPKM) value. Upregulated or downregulated genes in when comparing groups were identified by requiring a greater than 1.5-fold expression change and a false discovery rate (FDR) < 0.1, as well as a FPKM values > 1.0. The reproducibility of RNA-seq data was evaluated by applying the principal component analysis for all genes between biological replicates. UCSC genes from the iGenome mouse mm9 assembly (https://support.illumina.com/sequencing/sequencing_software/igenome.html) were used for gene annotation. Gene set enrichment and functional assignment were performed in software from the Broad Institute as described (***Martin et al., 2015***; ***Shan et al., 2017***; ***Subramanian et al., 2005***). Enrichment was evaluated for Day 31 CLP samples relative to Day 31 Sham samples.

ATAC-seq and data analysis

To determine the global impact of sepsis on chromatin accessibility, splenic memory P14 CD8 T cells were sorted from Sham and CLP hosts > 30 days after surgery. 5×10^4 cells were prepared for sequencing as previously described (***Buenrostro et al., 2015***; ***Shan et al., 2021***). The ATAC-seq data

are deposited at the GEO (accession number GSE174357) under the SuperSeries of GSE174359. The sequencing quality of ATAC-seq libraries was assessed by FastQC v0.11.4 (http://www.bioinformatics.babraham.ac.uk/projects/fastqc/) and adapters were removed through Cutadapt. The reads were mapped to mouse genome mm9 using Bowtie2 v2.2.5 and only uniquely mapped reads (MAPQ >10) were retained. The mapped reads from multiple replicates were pooled for Sham or CLP $CD8^+$ T cells, respectively, and were processed with MACS v2.1. 1 (***Zhang et al., 2008***) for peaks calling, with stringent criteria of ≥4 fold enrichment, *P*-value < 1E–five and FDR < 0.05. These sites were merged to generate a union pool of chromatin accessible sites containing 43,784 unique sites. For reproducibility analysis, reads at each site were counted in each ATAC-seq library, and then normalized by the total read-count of the union sites in the respective library. The resulting matrix was used for the principal component analysis. The read count matrix was used as input for edgeR (***Robinson et al., 2010***) (v.3.20.7.2) (quasi-likelihood test, robust, fold-change 2.0 and FDR < 0.01) to identify differential chromatin accessible sites between P14_Sham and P14_CLP conditions. A total of 304 Sham-specific and 1342 CLP-specific sites were identified, respectively.

CFSE

Splenocytes (10^7 /mL) from CLP and Sham hosts were labeled with CarboxyFluorescein diacetate Succinimidyl Ester (CFSE; eBioscience) by incubating the cells at room temperature for 15 minutes with 1 µM or 0.1 µM CFSE, respectively. Labeled cells were then incubated for 5 minutes with 1 mL FCS on ice to remove any free CFSE, and washed three times with RPMI prior to stimulation.

Peptide stimulation

CFSE labeled splenocytes from Sham and CLP hosts were mixed 1:1 and stimulated with 200 nM of GP_{33} peptide or media control for 8 hr at 37 °C in the presence of Brefeldin A (BfA; BD Biosciences).

Listeria challenge

Memory P14 CD8 T cells were isolated from either Sham or CLP hosts by positive selection, based on Thy1.1 expression, and naïve recipients received 2×10^5 of either P14 CD8 T cells each (controls did not receive cell transfer). Mice were subsequently infected the following day with 10^5 colony forming units (CFU) of virulent *Listeria monocytogenes* (10,403 s) express the GP_{33} epitope (*L.m.*-GP33).

Adhesion assay

Cellular adhesion was performed as previously described with some modification (***Bilal et al., 2015***; ***Chapman et al., 2012***). Briefly, flat-bottomed 96-well plates (Thermo-Fisher) were coated with 0–10 µg of αCD3 (OKT3, Biolegend). P14 CD8 T cells were isolated by positive selection, based on Thy1.1. 5×10^6 P14 CD8 T cells were incubated on the plate for 30 min. Non-adherent cells were removed by quickly inverting the plate to empty contents. Adherent cells were stained with αCD8a-APC-Cy7 (53–6.7; Biolegend). Cells were washed twice with PBS before being imaged utilizing Licor Odyssey Infrared detector.

TIRF microscopy

Images were taken using Leica AM TIRF MC imaging system as described with the following modifications (***Bilal et al., 2015***). P14 CD8 T cells were isolated by positive selection, based on Thy1.1, and placed on glass chamber slides (5×10^4 cells/chamber; LabTek II) precoated with 10 µg/mL α-CD3 mAb. Cells were stimulated for 15 minutes, fixed with 4 % paraformaldehyde, and permeabilized with 0.25 % Triton-X. Cells were blocked with SEA blocking buffer (Thermo-Fisher) for 1 hour and stained with 5 µL rabbit α-human/mouse AKT antibody (11E7, Cell Signaling Technology) overnight at 4 °C. Cells were washed and incubated with DyLight 488-conjugated donkey α-rabbit IgG (poly4064, BioLegend) secondary antibody for 2 hr at room temperature. Cells were washed and fresh PBS was added to each well. Images were taken at room temperature using 100 X oil submersion lens and Leica AM TIRF MC imaging system at the University of Iowa Central Microscopy Research Facility. Laser intensity and exposure parameters remained constant within each experiment. TIRF microscopy images were analyzed using ImageJ software. Membrane AKT was quantified by measuring mean pixel intensity in the longest axis of cells.

Statistical analysis

Unless stated otherwise data were analyzed using Prism8 software (GraphPad) using two-tailed Student t-test (for two individual groups, if unequal variance Mann-Whitney U test was used), one-way ANOVA with Bonferroni post-hoc test (for >2 individual groups, if unequal variance Kruskal-Wallis with Dunn's post-hoc test was used), two-way ANOVA (for multiparametric analysis of two or more individual groups, pairing was used for samples that came from the same animal), Fisher's exact test (for categorical data from two individual groups) with a confidence interval of >95% to determine significance (*$p \leq 0.05$). Data are presented as standard error of the mean.

Acknowledgements

We thank our labs and collaborators for their useful discussion. This work was supported by NIH Grants R01AI114543 (VPB), R21AI147064 (VPB), R35GM134880 (VPB), R21AI151183 (VPB), R01GM115462 (TSG), R35GM140881 (TSG), R01AI112579 (H-HX), R01AI121080 (H-HX and WP), R01AI139874 (H-HX and WP), R21AI157121 (JCH), T32AI007511 (IJJ), T32AI007485 (IJJ) and a Veterans Health Administration Merit Review Award I01B × 001324 (TSG). Research produced at the Central Microscopy Research Core at the University of Iowa was supported by the National Cancer Institute of the National Institutes of Health [P30CA086862].

Additional information

Funding

Funder	Grant reference number	Author
National Institutes of Health	R01AI114543	Vladimir P Badovinac
National Institutes of Health	R21AI147064	Vladimir P Badovinac
National Institutes of Health	R21AI151183	Vladimir P Badovinac
National Institutes of Health	R01GM115462	Thomas S Griffith
National Institutes of Health	R35GM134880	Vladimir P Badovinac
National Institutes of Health	R35GM140881	Thomas S Griffith
National Institutes of Health	R01AI112579	Hai-Hui Xue
National Institutes of Health	R01AI121080	Hai-Hui Xue Weiqun Peng
National Institutes of Health	R01AI139874	Hai-Hui Xue Weiqun Peng
National Institutes of Health	R21AI157121	Jon CD Houtman
National Institutes of Health	T32AI007511	Isaac J jensen
National Institutes of Health	T32AI007485	Isaac J jensen
Veterans Health Administration HSR and D	I0BX001324	Thomas S Griffith
National Cancer Institute	P30CA086862	Jon CD Houtman

Funder	Grant reference number	Author

The funders had no role in study design, data collection and interpretation, or the decision to submit the work for publication.

Author contributions

Isaac J Jensen, Conceptualization, Data curation, Formal analysis, Investigation, Methodology, Writing – original draft, Writing – review and editing; Xiang Li, Patrick W McGonagill, Data curation, Formal analysis, Writing – review and editing; Qiang Shan, Data curation, Methodology, Writing – review and editing; Micaela G Fosdick, Data curation, Formal analysis, Visualization, Writing – review and editing; Mikaela M Tremblay, Methodology, Writing – review and editing; Jon CD Houtman, Resources, Writing – review and editing; Hai-Hui Xue, Weiqun Peng, Resources, Supervision, Writing – review and editing; Thomas S Griffith, Writing – review and editing; Vladimir P Badovinac, Conceptualization, Funding acquisition, Resources, Supervision, Writing – review and editing

Author ORCIDs

Isaac J Jensen http://orcid.org/0000-0002-3107-3961
Micaela G Fosdick http://orcid.org/0000-0002-2427-532X
Hai-Hui Xue http://orcid.org/0000-0002-9163-7669
Thomas S Griffith http://orcid.org/0000-0002-7205-9859
Vladimir P Badovinac http://orcid.org/0000-0003-3180-2439

Ethics

Human subjects: Patients were recruited at the University of Iowa Hospitals and Clinics, an 811-bed academic tertiary care center. Blood sample acquisition, patient data collection, and analysis were approved by the University of Iowa Institutional Review Board (ID #201804822). Informed consent was obtained from patients or their legally authorized representatives.
Experimental procedures using mice were approved by University of Iowa Animal Care and Use Committee under ACURF protocol #6121915 and #9101915. The experiments performed followed Office of Laboratory Animal Welfare guidelines and PHS Policy on Humane Care and Use of Laboratory Animals. Cervical dislocation was used as the euthanasia method of all experimental mice. Inbred C57Bl/6 (B6, Thy1.2) and TCR-transgenic (TCR-Tg) P14 (Thy1.1) mice were purchased from the National Cancer Institute (Frederick, MD) and maintained in the animal facilities at the University of Iowa at the appropriate biosafety level according to the University of Iowa Animal Care and Use Committee and National Institutes of Health guidelines. Male and female mice >6 weeks of age were used for experiments; no discernable differences were observed based on sex of the animals.

Decision letter and Author response

Decision letter https://doi.org/10.7554/eLife.70989.sa1
Author response https://doi.org/10.7554/eLife.70989.sa2

Additional files

Supplementary files

- Transparent reporting form

Data availability

Sequencing data are deposited in GEO under accession code GSE174358. Source data for all figures are provided in associated excel files.

The following dataset was generated:

Author(s)	Year	Dataset title	Dataset URL	Database and Identifier
Peng B	2021	Sepsis leads to lasting changes in phenotype and function of memory CD8 T cells (RNA-Seq)	https://www.ncbi.nlm.nih.gov/geo/query/acc.cgi?acc=GSE174358	NCBI Gene Expression Omnibus, GSE174358

References

Badovinac VP, Haring JS, Harty JT. 2007. Initial T cell receptor transgenic cell precursor frequency dictates critical aspects of the CD8(+) T cell response to infection. *Immunity* **26**: 827–841. DOI: https://doi.org/10.1016/j.immuni.2007.04.013, PMID: 17555991

Baek KH, Shin HJ, Yoo JK, Cho JH, Choi YH, Sung YC, McKeon F, Lee CW. 2003. p53 deficiency and defective mitotic checkpoint in proliferating T lymphocytes increase chromosomal instability through aberrant exit from mitotic arrest. *Journal of Leukocyte Biology* **73**: 850–861. DOI: https://doi.org/10.1189/jlb.1202607, PMID: 12773518

Bilal MY, Zhang EY, Dinkel B, Hardy D, Yankee TM, Houtman JCD. 2015. GADS is required for TCR-mediated calcium influx and cytokine release, but not cellular adhesion, in human T cells. *Cellular Signalling* **27**: 841–850. DOI: https://doi.org/10.1016/j.cellsig.2015.01.012, PMID: 25636200

Borges da Silva H, Beura LK, Wang H, Hanse EA, Gore R, Scott MC, Walsh DA, Block KE, Fonseca R, Yan Y, Hippen KL, Blazar BR, Masopust D, Kelekar A, Vulchanova L, Hogquist KA, Jameson SC. 2018. The purinergic receptor P2RX7 directs metabolic fitness of long-lived memory CD8+ T cells. *Nature* **559**: 264–268. DOI: https://doi.org/10.1038/s41586-018-0282-0, PMID: 29973721

Buenrostro JD, Wu B, Chang HY, Greenleaf WJ. 2015. ATAC-seq: A Method for Assaying Chromatin Accessibility Genome-Wide. *Current Protocols in Molecular Biology* **109**: 21.. DOI: https://doi.org/10.1002/0471142727.mb2129s109

Cabrera-Perez J, Condotta SA, Badovinac VP, Griffith TS. 2014. Impact of sepsis on CD4 T cell immunity. *Journal of Leukocyte Biology* **96**: 767–777. DOI: https://doi.org/10.1189/jlb.5MR0114-067R, PMID: 24791959

Cabrera-Perez J, Condotta SA, James BR, Kashem SW, Brincks EL, Rai D, Kucaba TA, Badovinac VP, Griffith TS. 2015. Alterations in Antigen-Specific Naive CD4 T Cell Precursors after Sepsis Impairs Their Responsiveness to Pathogen Challenge. *Journal of Immunology* **194**: 1609–1620. DOI: https://doi.org/10.4049/jimmunol.1401711, PMID: 25595784

CDC. 2020. Sepsis: Data & Reports. https://www.cdc.gov/sepsis/datareports/index.html [Accessed August 1, 2020].

Chang JT, Wherry EJ, Goldrath AW. 2014. Molecular regulation of effector and memory T cell differentiation. *Nature Immunology* **15**: 1104–1115. DOI: https://doi.org/10.1038/ni.3031, PMID: 25396352

Chapman NM, Yoder AN, Houtman JCD. 2012. Non-Catalytic Functions of Pyk2 and Fyn Regulate Late Stage Adhesion in Human T Cells. *PLOS ONE* **7**: e53011. DOI: https://doi.org/10.1371/journal.pone.0053011, PMID: 23300847

Chen C-W, Mittal R, Klingensmith NJ, Burd EM, Terhorst C, Martin GS, Coopersmith CM, Ford ML. 2017. Cutting Edge: 2B4-Mediated Coinhibition of CD4+ T Cells Underlies Mortality in Experimental Sepsis. *Journal of Immunology* **199**: 1961–1966. DOI: https://doi.org/10.4049/jimmunol.1700375, PMID: 28768726

Cheung KP, Yang E, Goldrath AW. 2009. Memory-like CD8+ T cells generated during homeostatic proliferation defer to antigen-experienced memory cells. *Journal of Immunology* **183**: 3364–3372. DOI: https://doi.org/10.4049/jimmunol.0900641, PMID: 19675163

Cieri N, Camisa B, Cocchiarella F, Forcato M, Oliveira G, Provasi E, Bondanza A, Bordignon C, Peccatori J, Ciceri F, Lupo-Stanghellini MT, Mavilio F, Mondino A, Bicciato S, Recchia A, Bonini C. 2013. IL-7 and IL-15 instruct the generation of human memory stem T cells from naive precursors. *Blood* **121**: 573–584. DOI: https://doi.org/10.1182/blood-2012-05-431718, PMID: 23160470

Condotta SA, Rai D, James BR, Griffith TS, Badovinac VP. 2013. Sustained and incomplete recovery of naive CD8+ T cell precursors after sepsis contributes to impaired CD8+ T cell responses to infection. *Journal of Immunology* **190**: 1991–2000. DOI: https://doi.org/10.4049/jimmunol.1202379, PMID: 23355736

Condotta SA, Khan SH, Rai D, Griffith TS, Badovinac VP. 2015. Polymicrobial Sepsis Increases Susceptibility to Chronic Viral Infection and Exacerbates CD8+ T Cell Exhaustion. *Journal of Immunology* **195**: 116–125. DOI: https://doi.org/10.4049/jimmunol.1402473, PMID: 25980007

Danahy DB, Anthony SM, Jensen IJ, Hartwig SM, Shan Q, Xue HH, Harty JT, Griffith TS, Badovinac VP. 2017. Polymicrobial sepsis impairs bystander recruitment of effector cells to infected skin despite optimal sensing and alarming function of skin resident memory CD8 T cells. *PLOS Pathogens* **13**: e1006569. DOI: https://doi.org/10.1371/journal.ppat.1006569, PMID: 28910403

Danahy DB, Kurup SP, Winborn CS, Jensen IJ, Harty JT, Griffith TS, Badovinac VP. 2019. Sepsis-Induced State of Immunoparalysis Is Defined by Diminished CD8 T Cell-Mediated Antitumor Immunity. *Journal of Immunology* **203**: 725–735. DOI: https://doi.org/10.4049/jimmunol.1900435, PMID: 31189573

Davenport B, Eberlein J, van der Heide V, Jhun K, Nguyen TT, Victorino F, Trotta A, Chipuk J, Yi Z, Zhang W, Clambey ET, Scott DK, Homann D. 2019. Aging of Antiviral CD8+ Memory T Cells Fosters Increased Survival, Metabolic Adaptations, and Lymphoid Tissue Homing. *Journal of Immunology* **202**: 460–475. DOI: https://doi.org/10.4049/jimmunol.1801277, PMID: 30552164

Delano MJ, Ward PA. 2016a. The immune system's role in sepsis progression, resolution, and long-term outcome. *Immunological Reviews* **274**: 330–353. DOI: https://doi.org/10.1111/imr.12499, PMID: 27782333

Delano MJ, Ward PA. 2016b. Sepsis-induced immune dysfunction: can immune therapies reduce mortality? *The Journal of Clinical Investigation* **126**: 23–31. DOI: https://doi.org/10.1172/JCI82224, PMID: 26727230

Dombrovskiy VY, Martin AA, Sunderram J, Paz HL. 2007. Rapid increase in hospitalization and mortality rates for severe sepsis in the United States: a trend analysis from 1993 to 2003. *Critical Care Medicine* **35**: 1244–1250. DOI: https://doi.org/10.1097/01.CCM.0000261890.41311.E9, PMID: 17414736

Donnelly JP, Hohmann SF, Wang HE. 2015. Unplanned Readmissions After Hospitalization for Severe Sepsis at Academic Medical Center-Affiliated Hospitals. *Critical Care Medicine* **43**: 1916–1927. DOI: https://doi.org/10.1097/CCM.0000000000001147, PMID: 26082977

Duong S, Condotta SA, Rai D, Martin MD, Griffith TS, Badovinac VP. 2014. Polymicrobial Sepsis Alters Antigen-Dependent and -Independent Memory CD8 T Cell Functions. *Journal of Immunology* **192**: 3618–3625. DOI: https://doi.org/10.4049/jimmunol.1303460, PMID: 24646738

Ehl S, Hombach J, Aichele P, Hengartner H, Zinkernagel RM. 1997. Bystander Activation of Cytotoxic T Cells: Studies on the Mechanism and Evaluation of In Vivo Significance in a Transgenic Mouse Model. *The Journal of Experimental Medicine* **185**: 1241–1251. DOI: https://doi.org/10.1084/jem.185.7.1241, PMID: 9104811

Gaieski DF, Edwards JM, Kallan MJ, Carr BG. 2013. Benchmarking the incidence and mortality of severe sepsis in the United States. *Critical Care Medicine* **41**: 1167–1174. DOI: https://doi.org/10.1097/CCM.0b013e31827c09f8, PMID: 23442987

Gerlach C, Moseman EA, Loughhead SM, Alvarez D, Zwijnenburg AJ, Waanders L, Garg R, de la Torre JC, von Andrian UH. 2016. The Chemokine Receptor CX3CR1 Defines Three Antigen-Experienced CD8 T Cell Subsets with Distinct Roles in Immune Surveillance and Homeostasis. *Immunity* **45**: 1270–1284. DOI: https://doi.org/10.1016/j.immuni.2016.10.018, PMID: 27939671

Gurung P, Rai D, Condotta SA, Babcock JC, Badovinac VP, Griffith TS. 2011. Immune Unresponsiveness to Secondary Heterologous Bacterial Infection after Sepsis Induction Is TRAIL Dependent. *Journal of Immunology* **187**: 2148–2154. DOI: https://doi.org/10.4049/jimmunol.1101180, PMID: 21788440

Hotchkiss RS, Tinsley KW, Swanson PE, Schmieg RE Jr, Hui JJ, Chang KC, Osborne DF, Freeman BD, Cobb JP, Buchman TG, Karl IE. 2001. Sepsis-Induced Apoptosis Causes Progressive Profound Depletion of B and CD4+ T Lymphocytes in Humans. *Journal of Immunology* **166**: 6952–6963. DOI: https://doi.org/10.4049/jimmunol.166.11.6952, PMID: 11359857

Hotchkiss RS, Monneret G, Payen D. 2013. Sepsis-induced immunosuppression: from cellular dysfunctions to immunotherapy. *Nature Reviews. Immunology* **13**: 862–874. DOI: https://doi.org/10.1038/nri3552, PMID: 24232462

Hotchkiss RS, Moldawer LL, Opal SM, Reinhart K, Turnbull IR, Vincent JL. 2016. Sepsis and septic shock. *Nature Reviews. Disease Primers* **2**: 16045. DOI: https://doi.org/10.1038/nrdp.2016.45, PMID: 28117397

Hou H, Liu W, Wu S, Lu Y, Peng J, Zhu Y, Lu Y, Wang F, Sun Z, Lenz LL. 2014. Tim-3 Negatively Mediates Natural Killer Cell Function in LPS-Induced Endotoxic Shock. *PLOS ONE* **9**: e110585. DOI: https://doi.org/10.1371/journal.pone.0110585

Jensen IJ, Sjaastad FV, Griffith TS, Badovinac VP. 2018a. Sepsis-Induced T Cell Immunoparalysis: The Ins and Outs of Impaired T Cell Immunity. *Journal of Immunology* **200**: 1543–1553. DOI: https://doi.org/10.4049/jimmunol.1701618

Jensen IJ, Winborn CS, Fosdick MG, Shao P, Tremblay MM, Shan Q, Tripathy SK, Snyder CM, Xue H-H, Griffith TS, Houtman JC, Badovinac VP, Munz C. 2018b. Polymicrobial sepsis influences NK-cell-mediated immunity by diminishing NK-cell-intrinsic receptor-mediated effector responses to viral ligands or infections. *PLOS Pathogens* **14**: e1007405. DOI: https://doi.org/10.1371/journal.ppat.1007405

Jensen I.J, Jensen SN, Sjaastad FV, Gibson-Corley KN, Dileepan T, Griffith TS, Mangalam AK, Badovinac VP. 2020. Sepsis impedes EAE disease development and diminishes autoantigen-specific naive CD4 T cells. *eLife* **9**: e55800. DOI: https://doi.org/10.7554/eLife.55800, PMID: 33191915

Jensen I.J, McGonagill PW, Berton RR, Wagner BA, Silva EE, Buettner GR, Griffith TS, Badovinac VP. 2021a. Prolonged Reactive Oxygen Species Production following Septic Insult. *ImmunoHorizons* **5**: 477–488. DOI: https://doi.org/10.4049/immunohorizons.2100027

Jensen I.J, McGonagill PW, Butler NS, Harty JT, Griffith TS, Badovinac VP. 2021b. NK Cell–Derived IL-10 Supports Host Survival during Sepsis. *The Journal of Immunology* **206**: 1171–1180. DOI: https://doi.org/10.4049/jimmunol.2001131

Kaech SM, Cui W. 2012. Transcriptional control of effector and memory CD8+ T cell differentiation. *Nature Reviews. Immunology* **12**: 749–761. DOI: https://doi.org/10.1038/nri3307, PMID: 23080391

Kutza AST, Muhl E, Hackstein H, Kirchner H, Bein G. 1998. High Incidence of Active Cytomegalovirus Infection Among Septic Patients. *Clinical Infectious Diseases* **26**: 1076–1082. DOI: https://doi.org/10.1086/520307, PMID: 9597229

Lauer FT, Denson JL, Burchiel SW. 2017. Isolation, Cryopreservation, and Immunophenotyping of Human Peripheral Blood Mononuclear Cells. *Current Protocols in Toxicology* **74**: 18.. DOI: https://doi.org/10.1002/cptx.31, PMID: 29117436

Lertmemongkolchai G, Cai G, Hunter CA, Bancroft GJ. 2001. Bystander activation of CD8+ T cells contributes to the rapid production of IFN-gamma in response to bacterial pathogens. *Journal of Immunology* **166**: 1097–1105. DOI: https://doi.org/10.4049/jimmunol.166.2.1097, PMID: 11145690

Li H, Liu L, Zhang D, Xu J, Dai H, Tang N, Su X, Cao B. 2020. SARS-CoV-2 and viral sepsis: observations and hypotheses. *The Lancet* **395**: 1517–1520. DOI: https://doi.org/10.1016/S0140-6736(20)30920-X

Markwart R, Condotta SA, Requardt RP, Borken F, Schubert K, Weigel C, Bauer M, Griffith TS, Förster M, Brunkhorst FM, Badovinac VP, Rubio I. 2014. Immunosuppression after Sepsis: Systemic Inflammation and Sepsis Induce a Loss of Naïve T-Cells but No Enduring Cell-Autonomous Defects in T-Cell Function. *PLOS ONE* **9**: e115094. DOI: https://doi.org/10.1371/journal.pone.0115094, PMID: 25541945

Marshall JC. 2014. Why have clinical trials in sepsis failed? *Trends in Molecular Medicine* **20**: 195–203. DOI: https://doi.org/10.1016/j.molmed.2014.01.007, PMID: 24581450

Martin MD, Kim MT, Shan Q, Sompallae R, Xue HH, Harty JT, Badovinac VP. 2015. Phenotypic and Functional Alterations in Circulating Memory CD8 T Cells with Time after Primary Infection. *PLOS Pathogens* **11**: e1005219. DOI: https://doi.org/10.1371/journal.ppat.1005219, PMID: 26485703

Martin MD, Shan Q, Xue HH, Badovinac VP. 2017. Time and Antigen-Stimulation History Influence Memory CD8 T Cell Bystander Responses. *Frontiers in Immunology* **8**: 634. DOI: https://doi.org/10.3389/fimmu.2017.00634, PMID: 28642758

Martin MD, Badovinac VP. 2018. Defining Memory CD8 T Cell. *Frontiers in Immunology* **9**: 2692. DOI: https://doi.org/10.3389/fimmu.2018.02692, PMID: 30515169

Martin MD, Badovinac VP, Griffith TS. 2020. CD4 T Cell Responses and the Sepsis-Induced Immunoparalysis State. *Frontiers in Immunology* **11**: 1364. DOI: https://doi.org/10.3389/fimmu.2020.01364, PMID: 32733454

Masopust D, Vezys V, Marzo AL, Lefrançois L. 2001. Preferential Localization of Effector Memory Cells in Nonlymphoid Tissue. *Science* **291**: 2413–2417. DOI: https://doi.org/10.1126/science.1058867, PMID: 11264538

Milner JJ, Nguyen H, Omilusik K, Reina-Campos M, Tsai M, Toma C, Delpoux A, Boland BS, Hedrick SM, Chang JT, Goldrath AW. 2020. Delineation of a molecularly distinct terminally differentiated memory CD8 T cell population. *PNAS* **117**: 25667–25678. DOI: https://doi.org/10.1073/pnas.2008571117, PMID: 32978300

Mueller SN, Gebhardt T, Carbone FR, Heath WR. 2013. Memory T Cell Subsets, Migration Patterns, and Tissue Residence. *Annual Review of Immunology* **31**: 137–161. DOI: https://doi.org/10.1146/annurev-immunol-032712-095954, PMID: 23215646

Nolz JC, Harty JT. 2011. Protective Capacity of Memory CD8+ T Cells Is Dictated by Antigen Exposure History and Nature of the Infection. *Immunity* **34**: 781–793. DOI: https://doi.org/10.1016/j.immuni.2011.03.020, PMID: 21549619

Olson MR, McDermott DS, Varga SM. 2012. The Initial Draining Lymph Node Primes the Bulk of the CD8 T Cell Response and Influences Memory T Cell Trafficking after a Systemic Viral Infection. *PLOS Pathogens* **8**: e1003054. DOI: https://doi.org/10.1371/journal.ppat.1003054, PMID: 23236277

Palmer DC, Guittard GC, Franco Z, Crompton JG, Eil RL, Patel SJ, Ji Y, Van Panhuys N, Klebanoff CA, Sukumar M, Clever D, Chichura A, Roychoudhuri R, Varma R, Wang E, Gattinoni L, Marincola FM, Balagopalan L, Samelson LE, Restifo NP. 2015. Cish actively silences TCR signaling in CD8+ T cells to maintain tumor tolerance. *The Journal of Experimental Medicine* **212**: 2095–2113. DOI: https://doi.org/10.1084/jem.20150304, PMID: 26527801

Poehlmann H, Schefold JC, Zuckermann-Becker H, Volk HD, Meisel C. 2009. Phenotype changes and impaired function of dendritic cell subsets in patients with sepsis: a prospective observational analysis. *Critical Care* **13**: R119. DOI: https://doi.org/10.1186/cc7969, PMID: 19604380

Pribikova M, Moudra A, Stepanek O. 2018. Opinion: Virtual memory CD8 T cells and lymphopenia-induced memory CD8 T cells represent a single subset: Homeostatic memory T cells. *Immunology Letters* **203**: 57–61. DOI: https://doi.org/10.1016/j.imlet.2018.09.003, PMID: 30243945

Rai D, Pham NLL, Harty JT, Badovinac VP. 2009. Tracking the Total CD8 T Cell Response to Infection Reveals Substantial Discordance in Magnitude and Kinetics between Inbred and Outbred Hosts. *Journal of Immunology* **183**: 7672–7681. DOI: https://doi.org/10.4049/jimmunol.0902874, PMID: 19933864

Robinson MD, McCarthy DJ, Smyth GK. 2010. edgeR: a Bioconductor package for differential expression analysis of digital gene expression data. *Bioinformatics* **26**: 139–140. DOI: https://doi.org/10.1093/bioinformatics/btp616, PMID: 19910308

Roquilly A, McWilliam HEG, Jacqueline C, Tian Z, Cinotti R, Rimbert M, Wakim L, Caminschi I, Lahoud MH, Belz GT, Kallies A, Mintern JD, Asehnoune K, Villadangos JA. 2017. Local Modulation of Antigen-Presenting Cell Development after Resolution of Pneumonia Induces Long-Term Susceptibility to Secondary Infections. *Immunity* **47**: 135–147. DOI: https://doi.org/10.1016/j.immuni.2017.06.021, PMID: 28723546

Roquilly A, Jacqueline C, Davieau M, Mollé A, Sadek A, Fourgeux C, Rooze P, Broquet A, Misme-Aucouturier B, Chaumette T, Vourc'h M, Cinotti R, Marec N, Gauttier V, McWilliam HEG, Altare F, Poschmann J, Villadangos JA, Asehnoune K. 2020. Alveolar macrophages are epigenetically altered after inflammation, leading to long-term lung immunoparalysis. *Nature Immunology* **21**: 636–648. DOI: https://doi.org/10.1038/s41590-020-0673-x, PMID: 32424365

Rudd KE, Johnson SC, Agesa KM, Shackelford KA, Tsoi D, Kievlan DR, Colombara DV, Ikuta KS, Kissoon N, Finfer S, Fleischmann-Struzek C, Machado FR, Reinhart KK, Rowan K, Seymour CW, Watson RS, West TE, Marinho F, Hay SI, Lozano R, et al. 2020. Global, regional, and national sepsis incidence and mortality, 1990–2017: analysis for the Global Burden of Disease Study. *The Lancet* **395**: 200–211. DOI: https://doi.org/10.1016/S0140-6736(19)32989-7

Sariol A, Perlman S. 2020. Lessons for COVID-19 Immunity from Other Coronavirus Infections. *Immunity* **53**: 248–263. DOI: https://doi.org/10.1016/j.immuni.2020.07.005, PMID: 32717182

Sarkar I, Pati S, Dutta A, Basak U, Sa G. 2019. T-memory cells against cancer: Remembering the enemy. *Cellular Immunology* **338**: 27–31. DOI: https://doi.org/10.1016/j.cellimm.2019.03.002, PMID: 30928016

Schenkel JM, Fraser KA, Vezys V, Masopust D. 2013. Sensing and alarm function of resident memory CD8+ T cells. *Nature Immunology* **14**: 509–513. DOI: https://doi.org/10.1038/ni.2568, PMID: 23542740

Serbanescu MA, Ramonell KM, Hadley A, Margoles LM, Mittal R, Lyons JD, Liang Z, Coopersmith CM, Ford ML, McConnell KW. 2016. Attrition of memory CD8 T cells during sepsis requires LFA-1. *Journal of Leukocyte Biology* **100**: 1167–1180. DOI: https://doi.org/10.1189/jlb.4A1215-563RR, PMID: 27286793

Shan Q, Zeng Z, Xing S, Li F, Hartwig SM, Gullicksrud JA, Kurup SP, Van Braeckel-Budimir N, Su Y, Martin MD, Varga SM, Taniuchi I, Harty JT, Peng W, Badovinac VP, Xue H-H. 2017. The transcription factor Runx3 guards

cytotoxic CD8+ effector T cells against deviation towards follicular helper T cell lineage. *Nature Immunology* **18**: 931–939. DOI: https://doi.org/10.1038/ni.3773, PMID: 28604718

Shan Q, Hu S e, Chen X, Danahy DB, Badovinac VP, Zang C, Xue HH. 2021. Ectopic Tcf1 expression instills a stem-like program in exhausted CD8+ T cells to enhance viral and tumor immunity. *Cellular & Molecular Immunology* **18**: 1262–1277. DOI: https://doi.org/10.1038/s41423-020-0436-5, PMID: 32341523

Siegers GM, Barreira CR, Postovit LM, Dekaban GA. 2017. CD11d β2 integrin expression on human NK, B, and γδ T cells. *Journal of Leukocyte Biology* **101**: 1029–1035. DOI: https://doi.org/10.1189/jlb.3AB0716-326RR, PMID: 27881604

Singer M, Deutschman CS, Seymour CW, Shankar-Hari M, Annane D, Bauer M, Bellomo R, Bernard GR, Chiche J-D, Coopersmith CM, Hotchkiss RS, Levy MM, Marshall JC, Martin GS, Opal SM, Rubenfeld GD, van der Poll T, Vincent J-L, Angus DC. 2016. The Third International Consensus Definitions for Sepsis and Septic Shock (Sepsis-3). *JAMA* **315**: 801–810. DOI: https://doi.org/10.1001/jama.2016.0287, PMID: 26903338

Sjaastad FV, Condotta SA, Kotov JA, Pape KA, Dail C, Danahy DB, Kucaba TA, Tygrett LT, Murphy KA, Cabrera-Perez J, Waldschmidt TJ, Badovinac VP, Griffith TS. 2018. Polymicrobial Sepsis Chronic Immunoparalysis Is Defined by Diminished Ag-Specific T Cell-Dependent B Cell Responses. *Frontiers in Immunology* **9**: 2532. DOI: https://doi.org/10.3389/fimmu.2018.02532, PMID: 30429857

Sjaastad F.V, Jensen IJ, Berton RR, Badovinac VP, Griffith TS. 2020a. ducing Experimental Polymicrobial Sepsis by Cecal Ligation and Puncture. *Current Protocols in Immunology* **131**: e110. DOI: https://doi.org/10.1002/cpim.110

Sjaastad F.V, Kucaba TA, Dileepan T, Swanson W, Dail C, Cabrera-Perez J, Murphy KA, Badovinac VP, Griffith TS. 2020b. Polymicrobial Sepsis Impairs Antigen-Specific Memory CD4 T Cell-Mediated Immunity. *Frontiers in Immunology* **11**: 1786. DOI: https://doi.org/10.3389/fimmu.2020.01786, PMID: 32903436

Slütter B, Van Braeckel-Budimir N, Abboud G, Varga SM, Salek-Ardakani S, Harty JT. 2017. Dynamics of influenza-induced lung-resident memory T cells underlie waning heterosubtypic immunity. *Science Immunology* **2**: eaag2031. DOI: https://doi.org/10.1126/sciimmunol.aag2031, PMID: 28783666

Souza-Fonseca-Guimaraes F, Parlato M, Fitting C, Cavaillon JM, Adib-Conquy M. 2012. NK Cell Tolerance to TLR Agonists Mediated by Regulatory T Cells after Polymicrobial Sepsis. *Journal of Immunology* **188**: 5850–5858. DOI: https://doi.org/10.4049/jimmunol.1103616, PMID: 22566566

Strother RK, Danahy DB, Kotov DI, Kucaba TA, Zacharias ZR, Griffith TS, Legge KL, Badovinac VP. 2016. Polymicrobial Sepsis Diminishes Dendritic Cell Numbers and Function Directly Contributing to Impaired Primary CD8 T Cell Responses In Vivo. *Journal of Immunology* **197**: 4301–4311. DOI: https://doi.org/10.4049/jimmunol.1601463, PMID: 27798171

Subramanian A, Tamayo P, Mootha VK, Mukherjee S, Ebert BL, Gillette MA, Paulovich A, Pomeroy SL, Golub TR, Lander ES, Mesirov JP. 2005. Gene set enrichment analysis: A knowledge-based approach for interpreting genome-wide expression profiles. *PNAS* **102**: 15545–15550. DOI: https://doi.org/10.1073/pnas.0506580102, PMID: 16199517

Trapnell C, Pachter L, Salzberg SL. 2009. TopHat: discovering splice junctions with RNA-Seq. *Bioinformatics* **25**: 1105–1111. DOI: https://doi.org/10.1093/bioinformatics/btp120, PMID: 19289445

Unsinger J, Kazama H, McDonough JS, Hotchkiss RS, Ferguson TA. 2009. Differential lymphopenia-induced homeostatic proliferation for CD4+ and CD8+ T cells following septic injury. *Journal of Leukocyte Biology* **85**: 382–390. DOI: https://doi.org/10.1189/jlb.0808491, PMID: 19088177

Unsinger J, Kazama H, McDonough JS, Griffith TS, Hotchkiss RS, Ferguson TA. 2010. Sepsis-Induced Apoptosis Leads to Active Suppression of Delayed-Type Hypersensitivity by CD8+ Regulatory T Cells through a TRAIL-Dependent Mechanism. *Journal of Immunology* **184**: 6766–6772. DOI: https://doi.org/10.4049/jimmunol.0904054, PMID: 20483771

Van Gassen S, Callebaut B, Van Helden MJ, Lambrecht BN, Demeester P, Dhaene T, Saeys Y. 2015. FlowSOM: Using self-organizing maps for visualization and interpretation of cytometry data. *Cytometry. Part A* **87**: 636–645. DOI: https://doi.org/10.1002/cyto.a.22625, PMID: 25573116

Walton AH, Muenzer JT, Rasche D, Boomer JS, Sato B, Brownstein BH, Pachot A, Brooks TL, Deych E, Shannon WD, Green JM, Storch GA, Hotchkiss RS. 2014. Reactivation of Multiple Viruses in Patients with Sepsis. *PLOS ONE* **9**: e98819. DOI: https://doi.org/10.1371/journal.pone.0098819, PMID: 24919177

Wherry EJ, Teichgräber V, Becker TC, Masopust D, Kaech SM, Antia R, von Andrian UH, Ahmed R. 2003. Lineage relationship and protective immunity of memory CD8 T cell subsets. *Nature Immunology* **4**: 225–234. DOI: https://doi.org/10.1038/ni889, PMID: 12563257

White JT, Cross EW, Kedl RM. 2017. Antigen-inexperienced memory CD8+ T cells: where they come from and why we need them. *Nature Reviews. Immunology* **17**: 391–400. DOI: https://doi.org/10.1038/nri.2017.34, PMID: 28480897

Xie J, Chen C -w, Sun Y, Laurie SJ, Zhang W, Otani S, Martin GS, Coopersmith CM, Ford ML. 2019. creased attrition of memory T cells during sepsis requires 2B4. *JCI Insight* **4**: e126030. DOI: https://doi.org/10.1172/jci.insight.126030

Yamamoto A, Taki T, Yagi H, Habu T, Yoshida K, Yoshimura Y, Yamamoto K, Matsushiro A, Nishimune Y, Morita T. 1996. Cell cycle-dependent expression of the mouse Rad51 gene in proliferating cells. *Molecular & General Genetics* **251**: 1–12. DOI: https://doi.org/10.1007/BF02174338, PMID: 8628240

Zhang Y, Liu T, Meyer CA, Eeckhoute J, Johnson DS, Bernstein BE, Nusbaum C, Myers RM, Brown M, Li W, Liu XS. 2008. Model-based analysis of ChIP-Seq (MACS). *Genome Biology* **9**: R137. DOI: https://doi.org/10.1186/gb-2008-9-9-r137, PMID: 18798982